

# Transformation texture and Orientation relationship

Vahid Tari, Ben Anglin, S. Mandal, and A.D. Rollett

27-750

Texture, Microstructure & Anisotropy

Last revised 28<sup>th</sup> Apr. 2016



# Objective

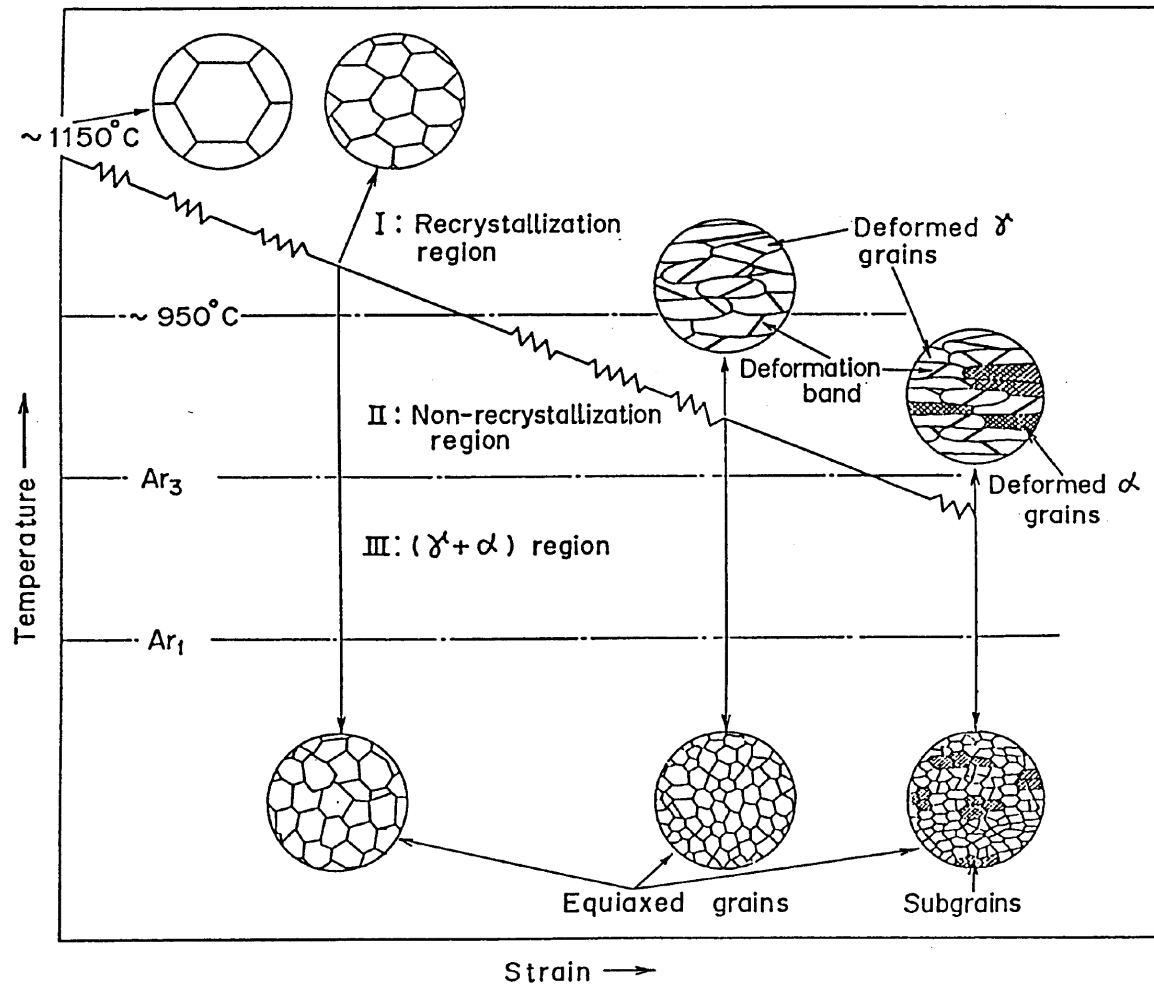
- Understand orientation relationships
- Phase transformation and variant selection in steel alloys
- Phase transformation and variant selection in Titanium alloys
- Construct misorientation matrices from given orientation relationship
- Forward and backward texture prediction



# Orientation Relationships

- Orientation Relationship (OR): Relation between specific planes and directions of two crystals on either side of boundary.
- During most phase transformations, some favored orientation relationship exists between the parent and the product phases which allows the best fit at the interface between the two crystals.
- Why important? Phase transformations; morphology of precipitates; nucleation mechanisms; interfaces; high temperature orientation determination; thin film orientation prediction.

# Why transformation texture and OR are important?



- Ray and Jonas, International Materials Reviews 1990 Vol. 35 NO.1



# Orientation relationship (OR)

Notation:

$$(hkl)_{\alpha} // (h'k'l')_{\beta} \quad [uvw]_{\alpha} // [u'v'w']_{\beta}$$

The  $(hkl)$  plane of the  $\alpha$  crystal lies parallel to the  $(h'k'l')$  plane of the  $\beta$  crystal

Similarly for the  $[uvw]$  and  $[u'v'w']$  directions of the two crystals

$[uvw]$  and  $[u'v'w']$  must lie in the  $(hkl)$  and  $(h'k'l')$  planes, respectively

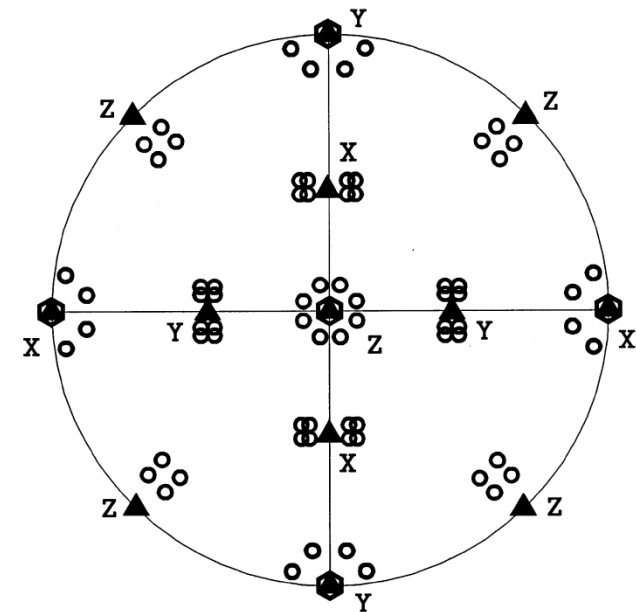
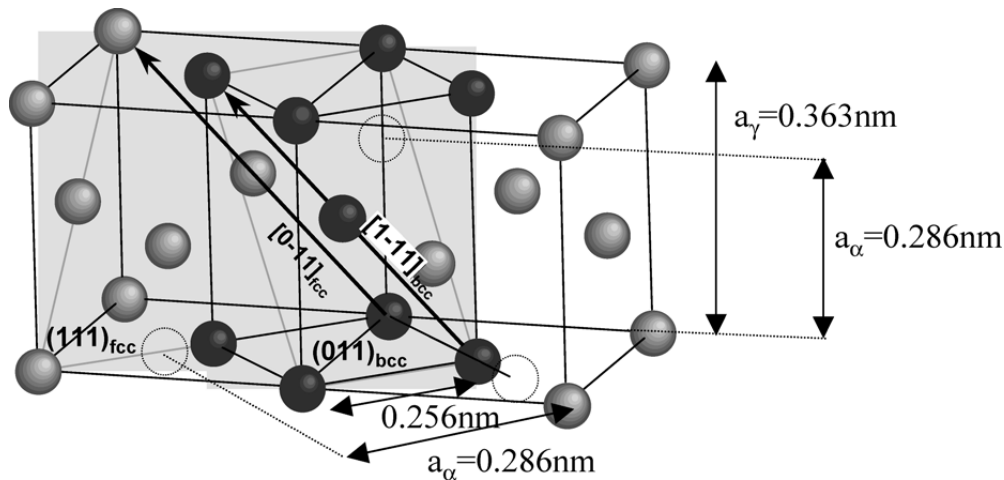
The orientation relationship holds regardless of the coherency of the boundary

# OR Variants

Variants of a given OR are specific alignment of planes and directions. These exist because of crystal symmetry

In the K-S OR, there are 4  $\{111\}_\gamma$  planes, each plane parallel to a  $\{110\}_\alpha$  plane. A  $\{111\}_\gamma$  plane contains 3  $\langle 110 \rangle_\gamma$  directions and each  $\langle 110 \rangle_\gamma$  direction is parallel to 2  $\langle 111 \rangle_\alpha$  directions [1]. Hence 24 K-S variants.

$$\begin{aligned} [1 \ 1 \ 1]_\gamma &\parallel [0 \ 1 \ 1]_\alpha \\ [\bar{1} \ 0 \ 1]_\gamma &\parallel [\bar{1} \ \bar{1} \ 1]_\alpha \\ [1 \ \bar{2} \ 1]_\gamma &\parallel [2 \ \bar{1} \ 1]_\alpha \end{aligned}$$



- ◻ Starting Orientation (1)
- ▲ Bain Variant (3)
- K-S Variant (24)

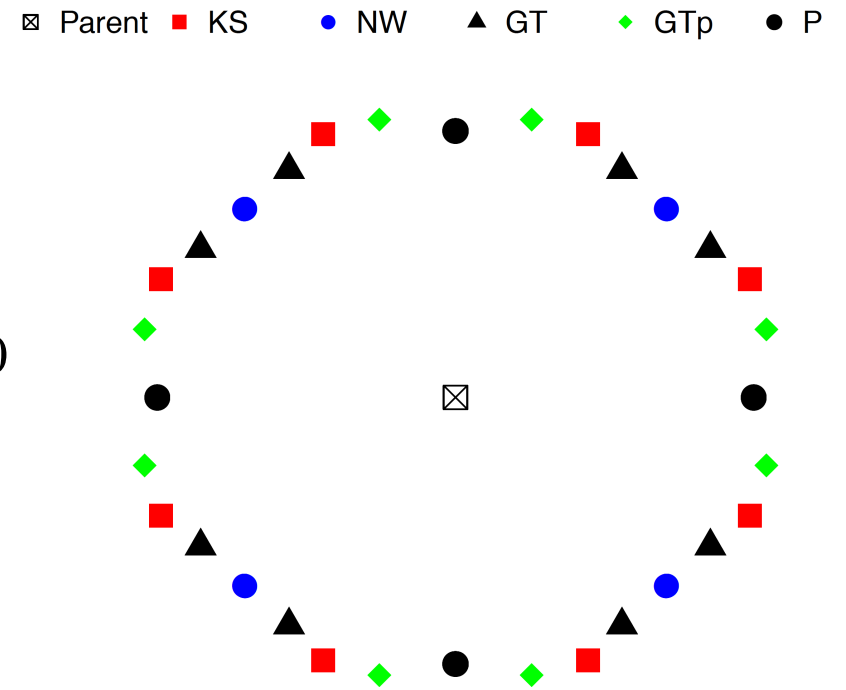
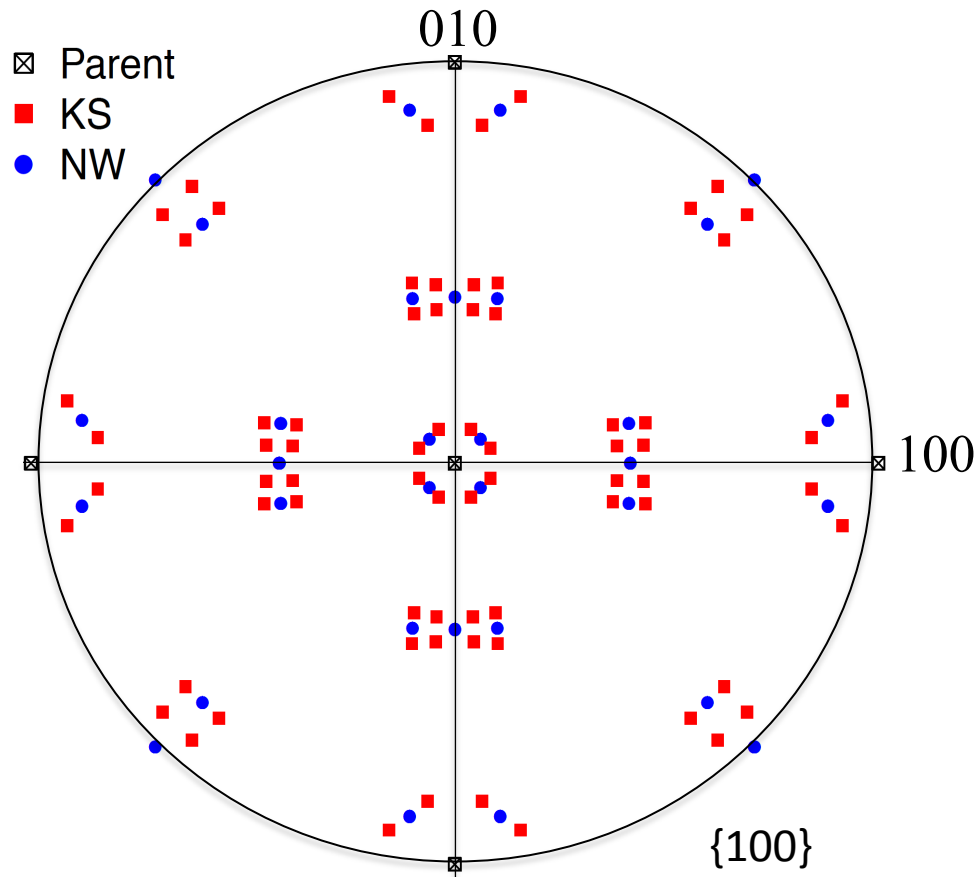
# Orientation relationships in Steel

---

Orientation relationship	Parallelism
Pitsch (P)	$\{100\}_\gamma // \{011\}_\alpha$ $\langle 011 \rangle_\gamma // \langle 111 \rangle_\alpha$
Nishiyama–Wasserman (N–W)	$\{111\}_\gamma // \{110\}_\alpha$ $\langle 112 \rangle_\gamma // \langle 110 \rangle_\alpha$
Kurdjumov–Sachs (K–S)	$\{111\}_\gamma // \{110\}_\alpha$ $\langle 110 \rangle_\gamma // \langle 111 \rangle_\alpha$
Greninger–Troiano (G–T)	$\{111\}_\gamma // \{110\}_\alpha$ $\langle 123 \rangle_\gamma // \langle 133 \rangle_\alpha$
Greninger–Troiano' (G–T')	$\{110\}_\gamma // \{111\}_\alpha$ $\langle 133 \rangle_\gamma // \langle 123 \rangle_\alpha$

---

# Stereographic Projection of ORs



# Variants Selection

- Variants selection: Few of the theoretically predicted variants dominant. Some variants may be preferred over others depending on the transformation mechanism.
- Knowledge about variants selection important to understand microstructure evolution.

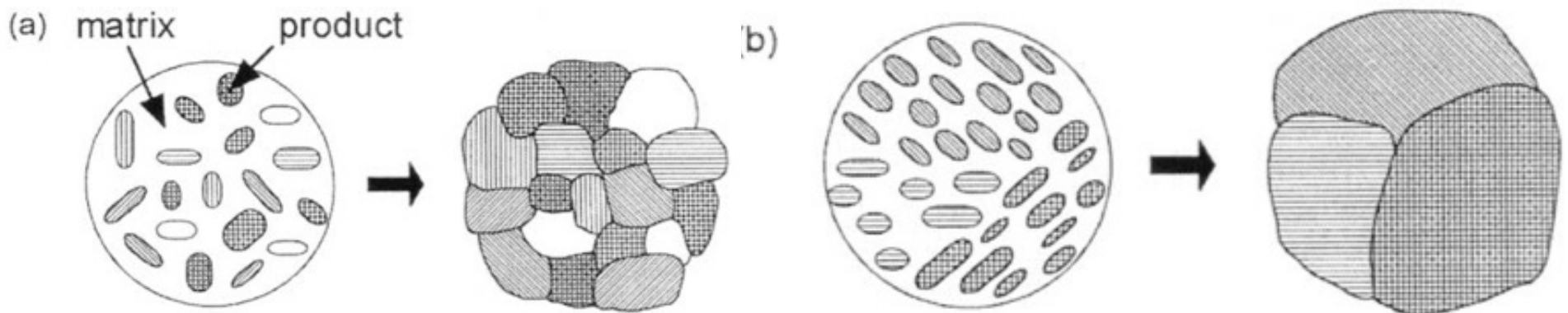
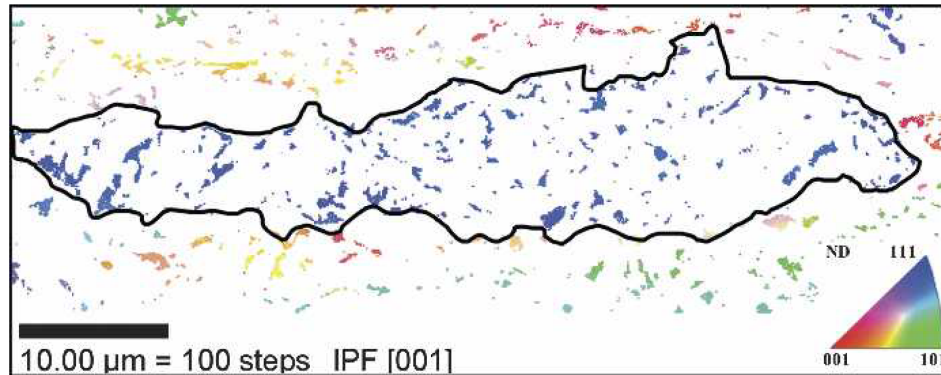


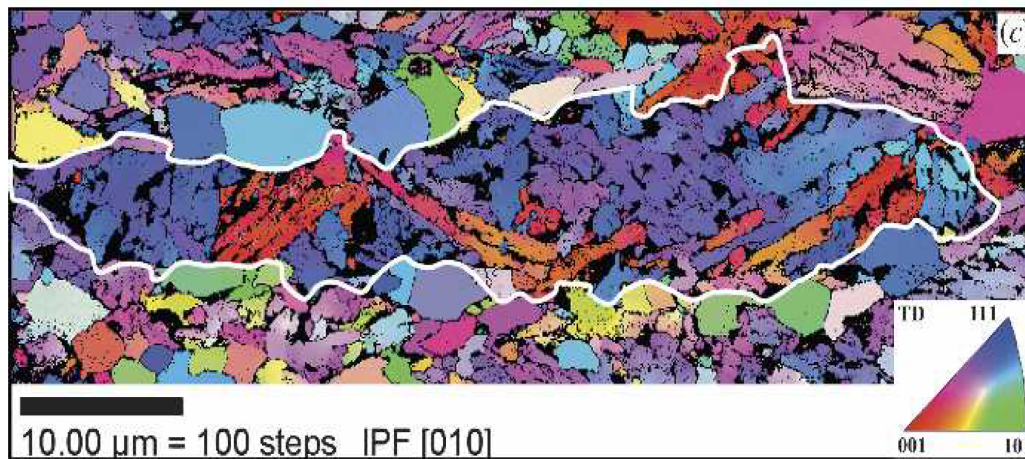
Fig: Evolution of microstructure during diffusional phase transformation (a) without variant selection (each nucleus with a different variant becomes a different grain, resulting in a fine structure). (b) with variant selection (neighboring nuclei having the same variants coalesce to form larger grains). (Furuhara and Maki, 2001)



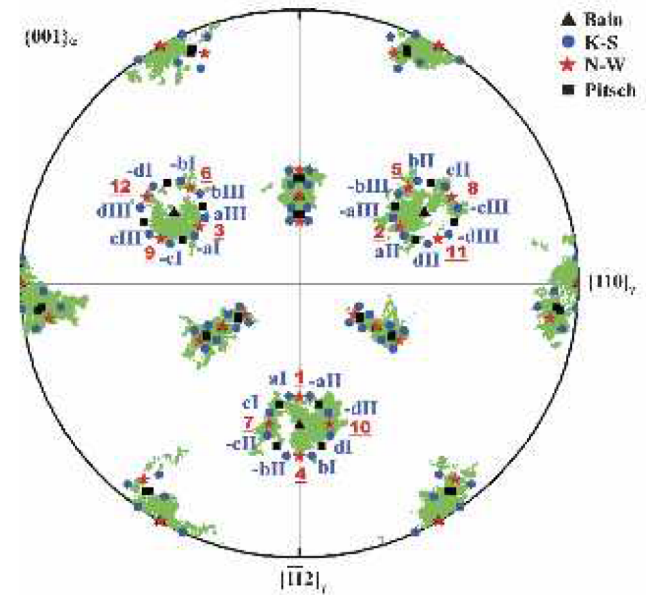
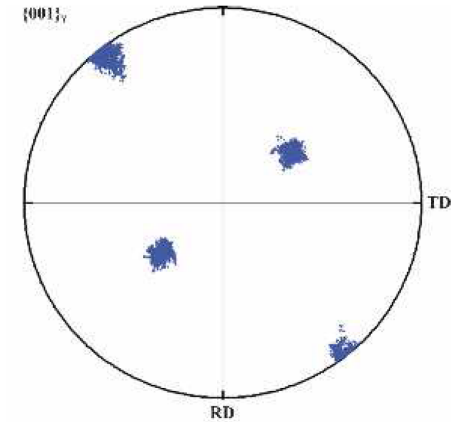
# Variant selection during phase transformation in steel



(a)

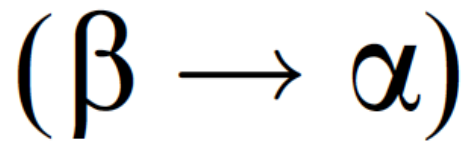


(c)



- Youliang He, John J Jonas, Stéphane Godet, Metallurgical and Materials Transactions A, Vol. 37A, 2006,2641

# OR (Burgers) in Titanium Alloys



Phase transformation  
BCC  $\longrightarrow$  HCP

- Predominant OR observed for body-centered cubic to hexagonal transformation in Ti alloys
- Burgers OR

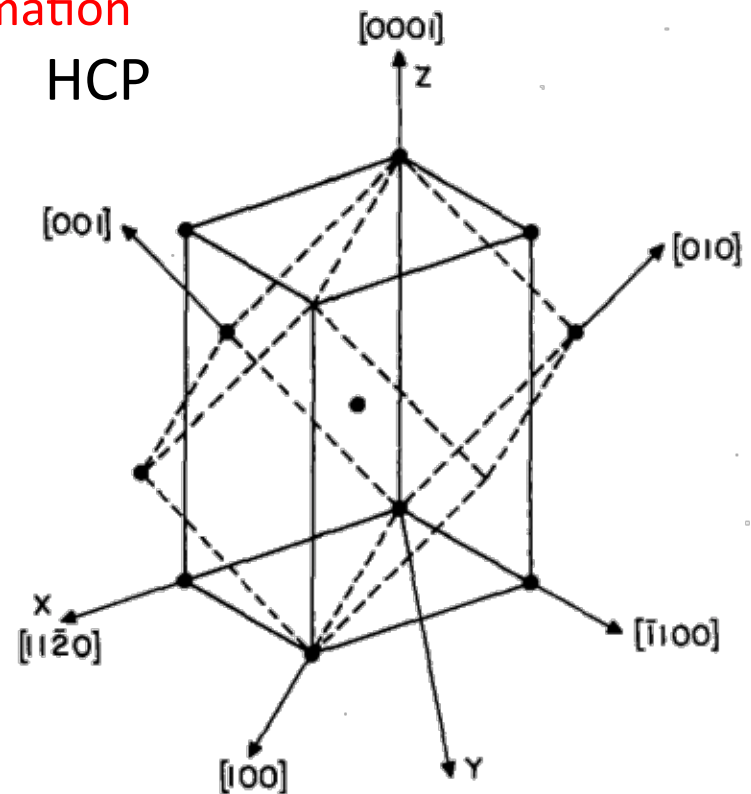


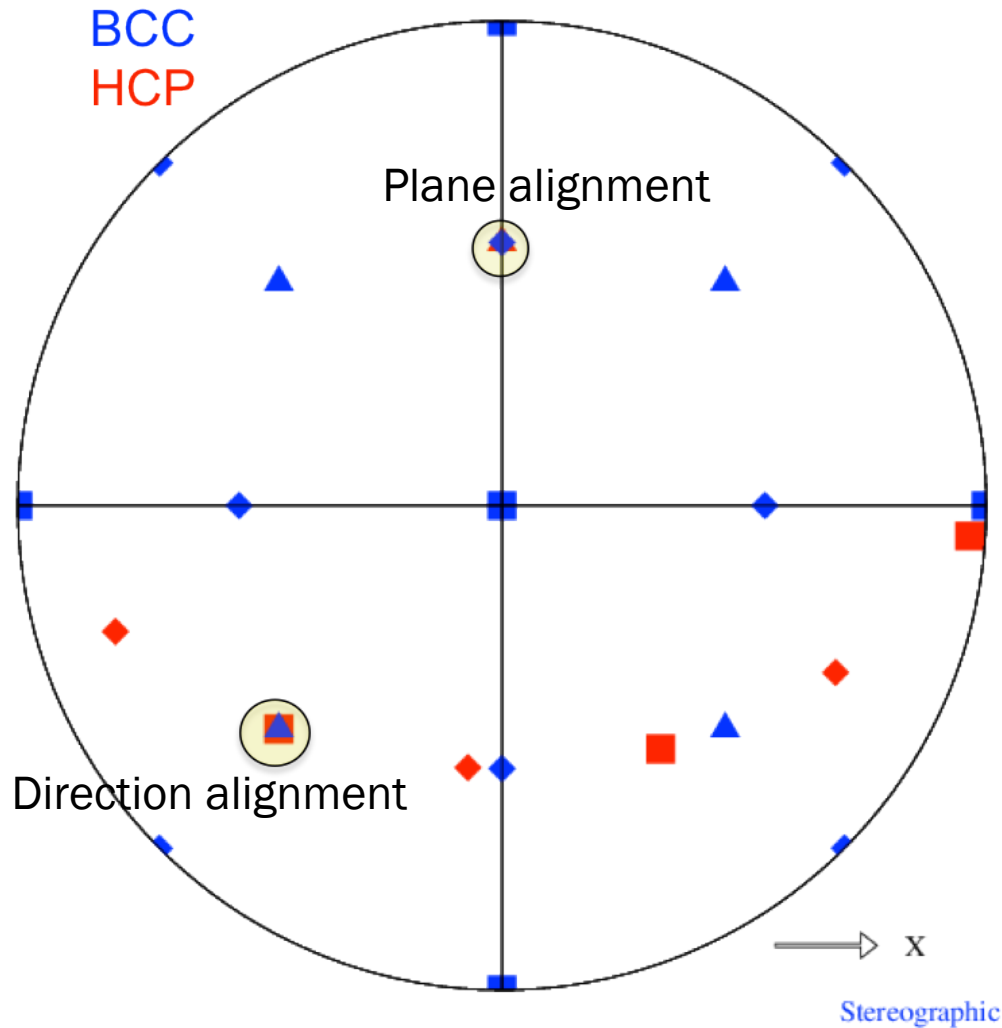
Fig: Geometrical representation of the Burgers OR with dashed lines showing the BCC crystal and continuous lines showing the HCP crystal (Menon et al.,1986)

# Burgers OR Variants







- Variants: Each crystallographic orientation relationship predicts different numbers of product orientations originating from a single crystallographic orientation of the parent phase.
- Number of variants is determined by the OR that the product phase have with the parent phase.
- # variants for Burger's OR=12

Variant	Plane parallel	Direction parallel
V1	$(1 \bar{1} 0)_\beta \parallel (0 0 0 1)_\alpha$	$[1 1 1]_\beta \parallel [1 1 \bar{2} 0]_\alpha$
V2	$(1 0 \bar{1})_\beta \parallel (0 0 0 1)_\alpha$	$[1 1 1]_\beta \parallel [1 1 \bar{2} 0]_\alpha$
V3	$(0 1 \bar{1})_\beta \parallel (0 0 0 1)_\alpha$	$[1 1 1]_\beta \parallel [1 1 \bar{2} 0]_\alpha$
V4	$(1 1 0)_\beta \parallel (0 0 0 1)_\alpha$	$[\bar{1} 1 1]_\beta \parallel [1 1 \bar{2} 0]_\alpha$
V5	$(1 0 1)_\beta \parallel (0 0 0 1)_\alpha$	$[\bar{1} 1 1]_\beta \parallel [1 1 \bar{2} 0]_\alpha$
V6	$(0 1 \bar{1})_\beta \parallel (0 0 0 1)_\alpha$	$[\bar{1} 1 1]_\beta \parallel [1 1 \bar{2} 0]_\alpha$
V7	$(1 1 0)_\beta \parallel (0 0 0 1)_\alpha$	$[1 \bar{1} 1]_\beta \parallel [1 1 \bar{2} 0]_\alpha$
V8	$(1 0 \bar{1})_\beta \parallel (0 0 0 1)_\alpha$	$[1 \bar{1} 1]_\beta \parallel [1 1 \bar{2} 0]_\alpha$
V9	$(0 1 1)_\beta \parallel (0 0 0 1)_\alpha$	$[1 \bar{1} 1]_\beta \parallel [1 1 \bar{2} 0]_\alpha$
V10	$(1 \bar{1} 0)_\beta \parallel (0 0 0 1)_\alpha$	$[1 1 \bar{1}]_\beta \parallel [1 1 \bar{2} 0]_\alpha$
V11	$(1 0 1)_\beta \parallel (0 0 0 1)_\alpha$	$[1 1 \bar{1}]_\beta \parallel [1 1 \bar{2} 0]_\alpha$
V12	$(0 1 1)_\beta \parallel (0 0 0 1)_\alpha$	$[1 1 \bar{1}]_\beta \parallel [1 1 \bar{2} 0]_\alpha$

# Stereographic Projection of Burgers OR

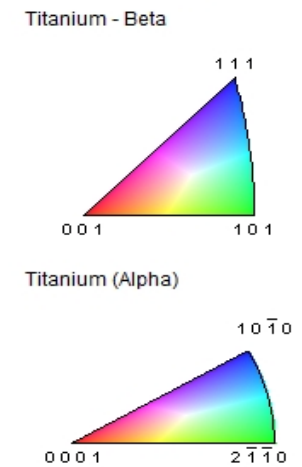
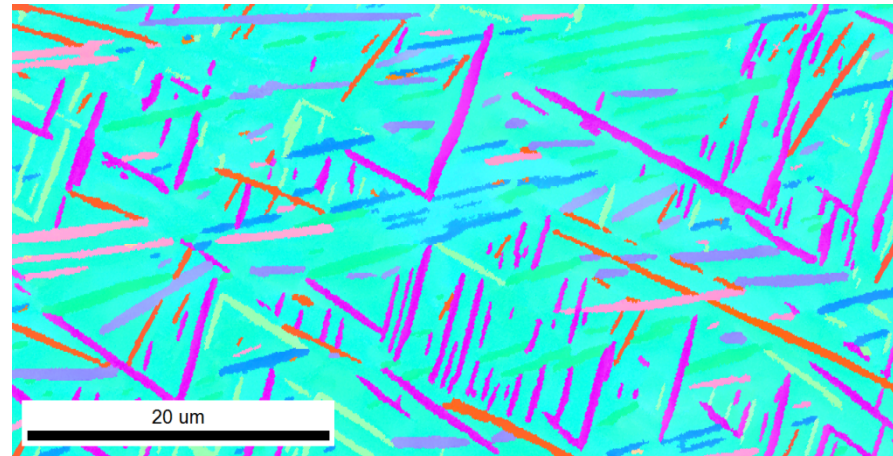


Stereographic projection for one of the variants of the Burgers OR with a parent BCC orientation of  $\{0,0,0\}$ . Constructed using in-house scripts *OR stereogram* and *DrawPF*. Available from AD Rollett.

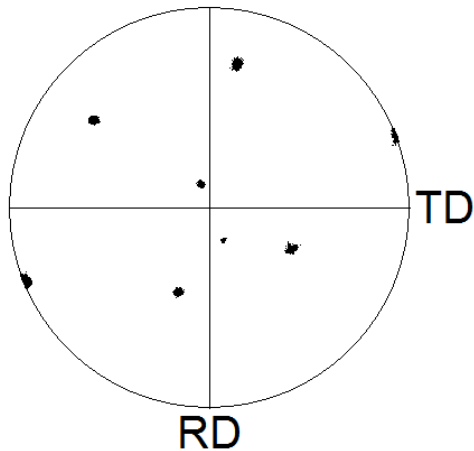
BCC (high T)		Hexagonal (low T)	
	111		0001
	100		11-20
	110		10-10

# An example

Fig: IPF map of an EBSD dataset.  
(Provided by IISc)



Titanium (Alpha)  
0 0 0 1



Titanium - Beta  
1 1 0

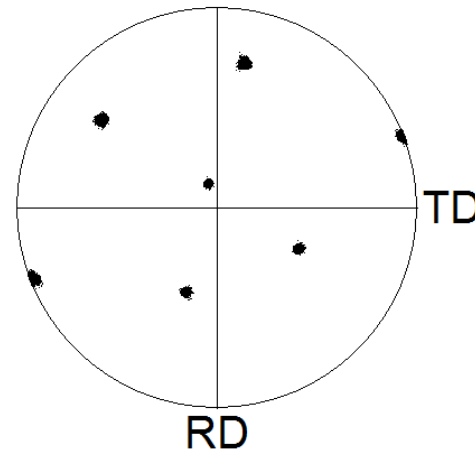


Fig: Pole figures generated using TSL software for this data.

# Variants Selection in Ti

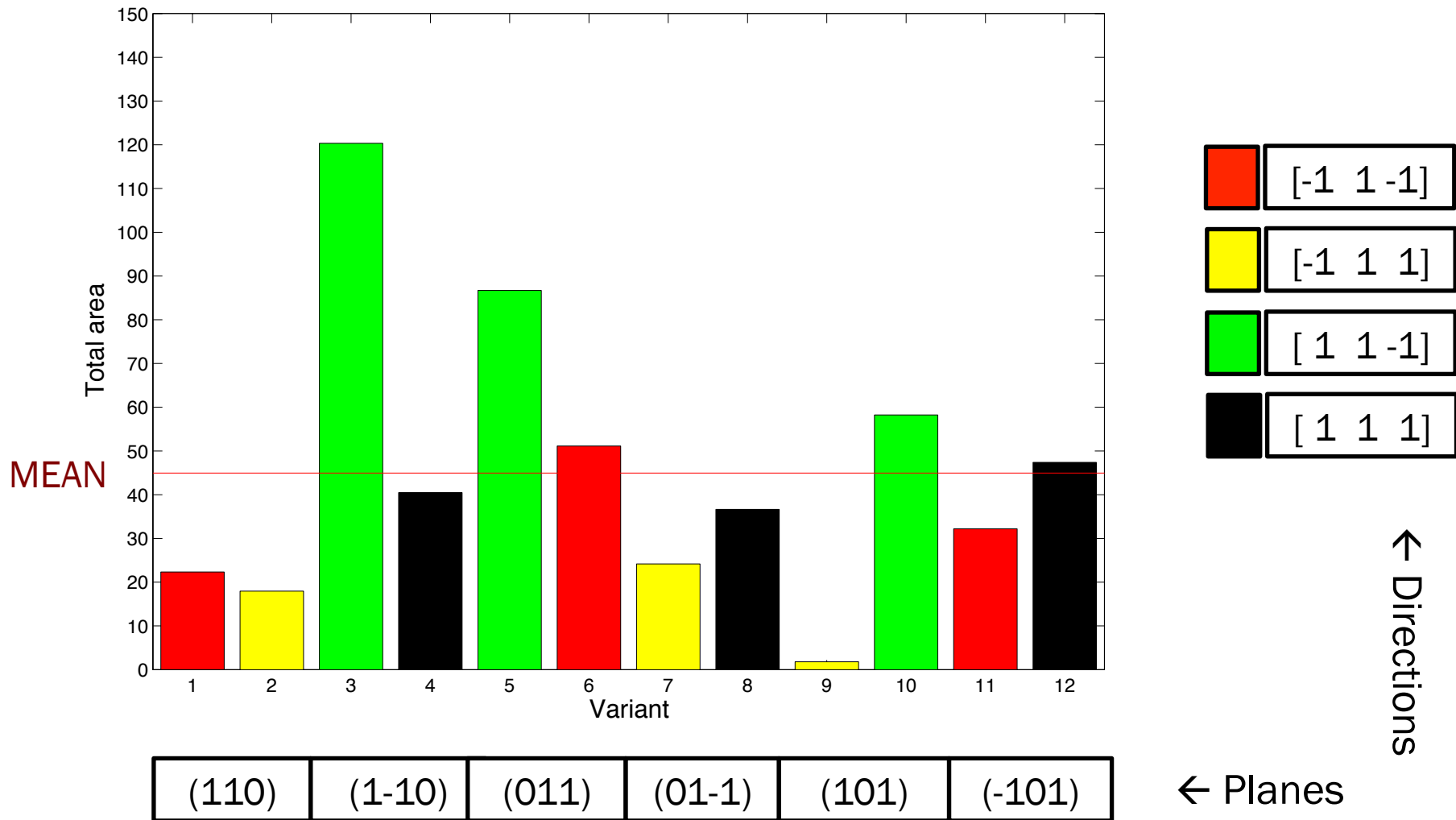


Fig: Relative frequency of variants for the EBSD dataset (Provided by IISC).

# Creating Misorientation Matrix for OR

$$[u \ v \ w]_{\alpha} \parallel [u' \ v' \ w']_{\beta} \quad (h \ k \ l)_{\alpha} \parallel (h' \ k' \ l')_{\beta}$$

Assume:  $(hkl) // (h'k'l') // ND$

and  $[uvw] // [u'v'w'] // RD$

$$g_{\alpha} = \begin{pmatrix} b_1 & t_1 & n_1 \\ b_2 & t_2 & n_2 \\ b_3 & t_3 & n_3 \end{pmatrix}$$

1.) Construct orientation matrix for phase  $\alpha$ .

2.) Construct orientation matrix for phase  $\beta$ .

$$g_{\beta} = \begin{pmatrix} b'_1 & t'_1 & n'_1 \\ b'_2 & t'_2 & n'_2 \\ b'_3 & t'_3 & n'_3 \end{pmatrix}$$

3.) Compute misorientation matrix from the  $\alpha$  phase to the  $\beta$  phase.

Note the importance of the sense of the transformation; for grain boundaries we invoke switching symmetry but you must *not* apply this to phase transformations!

$$\Delta g = g_{\beta} g_{\alpha}^{-1}$$



# Creating Misorientation Matrix for OR

Consider the K-S orientation relationship:

$$\begin{array}{l} (111)_{fcc} \parallel (-110)_{bcc} \\ [1-10]_{fcc} \parallel [111]_{bcc} \end{array}$$

- 1) Construct orientation matrix for phase *fcc*.
- 2) Construct orientation matrix for phase *bcc*.
- 3) Compute misorientation matrix from one phase to the other; here we pass from *fcc* (high temperature) to *bcc* (low temperature).

$$\Delta g = g_{bcc} g_{fcc}^{-1}$$

$$Q_{KS} = \frac{1}{6} \begin{bmatrix} 1 & 1 + 2\sqrt{6} & -2 + \sqrt{6} \\ 1 - 2\sqrt{6} & 1 & -2 - \sqrt{6} \\ -2 - \sqrt{6} & -2 + \sqrt{6} & 4 \end{bmatrix}$$



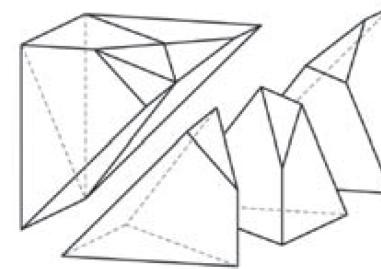
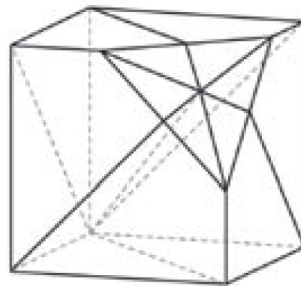
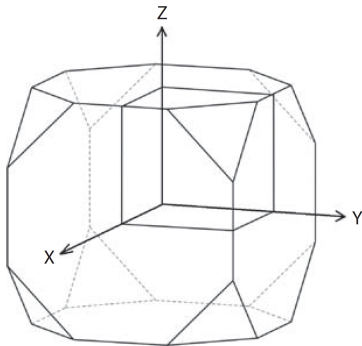
# Minimum misorientation angle and axis associated with ORs

$$\Delta g = g_{bcc} g_{fcc}^{-1}$$

$$Q_{KS} = \frac{1}{6} \begin{bmatrix} 1 & 1+2\sqrt{6} & -2+\sqrt{6} \\ 1-2\sqrt{6} & 1 & -2-\sqrt{6} \\ -2-\sqrt{6} & -2+\sqrt{6} & 4 \end{bmatrix}$$

$$T = \Delta g = O_{bcc} g_{bcc} (O_{fcc} g_{fcc})^{-1}$$

$$T = \Delta g = O_{bcc} g_{bcc} g_{fcc}^{-1} O_{fcc} \quad Q_{KS} = \frac{1}{6} \begin{bmatrix} 1+2\sqrt{6} & 2-\sqrt{6} & 1 \\ 1 & 2+\sqrt{6} & 1-2\sqrt{6} \\ 2-\sqrt{6} & 4 & 2+\sqrt{6} \end{bmatrix}$$



## Minimum misorientation angle and axis associated with ORs

Orientation relationship	Parallelism	Minimum angle/axis	No. of variants
Pitsch (P)	$\{100\}\gamma//\{011\}\alpha$ $\langle 011 \rangle\gamma//\langle 111 \rangle\alpha$	$45.98^\circ \langle 0.083 \ 0.201 \ 0.976 \rangle$	12
Nishiyama–Wasserman (N–W)	$\{111\}\gamma//\{110\}\alpha$ $\langle 112 \rangle\gamma//\langle 110 \rangle\alpha$	$45.98^\circ \langle 0.976 \ 0.083 \ 0.201 \rangle$	12
Kurdjumov–Sachs (K–S)	$\{111\}\gamma//\{110\}\alpha$ $\langle 110 \rangle\gamma//\langle 111 \rangle\alpha$	$42.85^\circ \langle 0.968 \ 0.178 \ 0.178 \rangle$	24
Greninger–Troiano (G–T)	$\{111\}\gamma//\{110\}\alpha$ $\langle 123 \rangle\gamma//\langle 133 \rangle\alpha$	$44.23^\circ \langle 0.973 \ 0.189 \ 0.133 \rangle$	24
Greninger–Troiano' (G–T')	$\{110\}\gamma//\{111\}\gamma$ $\langle 133 \rangle\gamma//\langle 123 \rangle\alpha$	$44.23^\circ \langle 0.189 \ 0.973 \ 0.133 \rangle$	24

# ORs in Rodrigues space

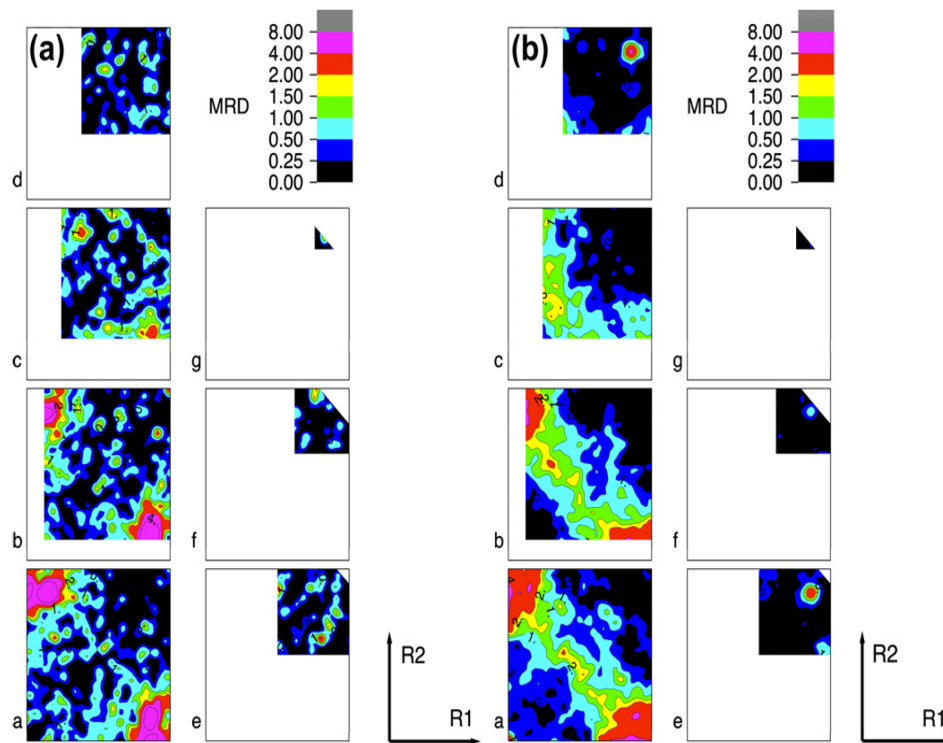


Fig. 8. MD between Cu and Nb in terms of the Rodrigues–Frank vector space  $\mathbf{R}(R_1, R_2, R_3)$  For (a) the PVD sample and (b) the CANb92 sample. Note that the two phase MD is in principle different for each phase, in contrast to grain boundary MD, although in the data presented here the differences are minor. Both samples show strong peaks of well-known misorientation relationships between fcc and bcc metals, such as the Kurdjumov–Sachs, Nishiyama–Wasserman, Bain and/or Pitsch relationships.

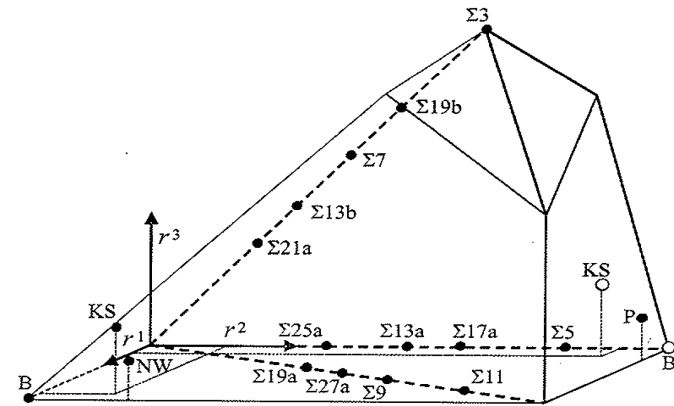
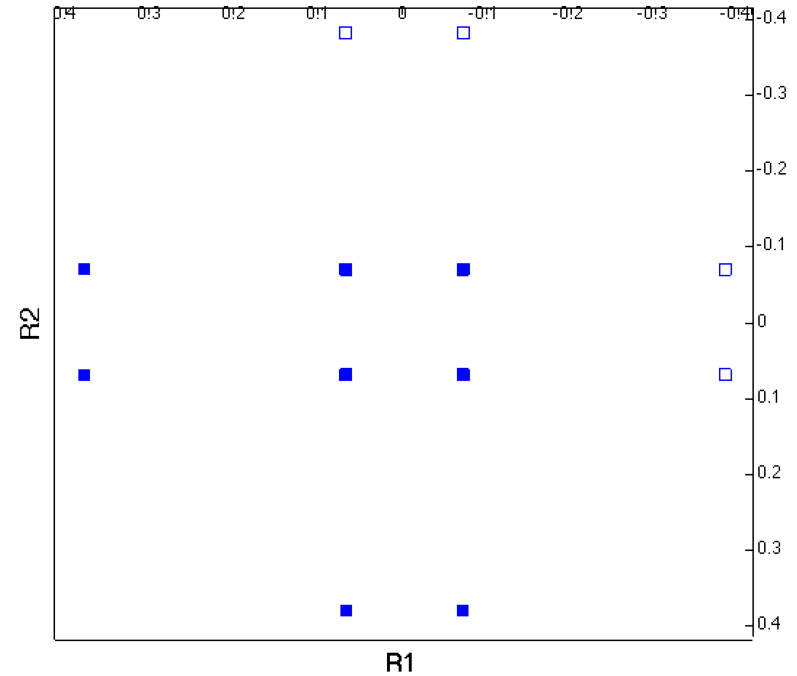
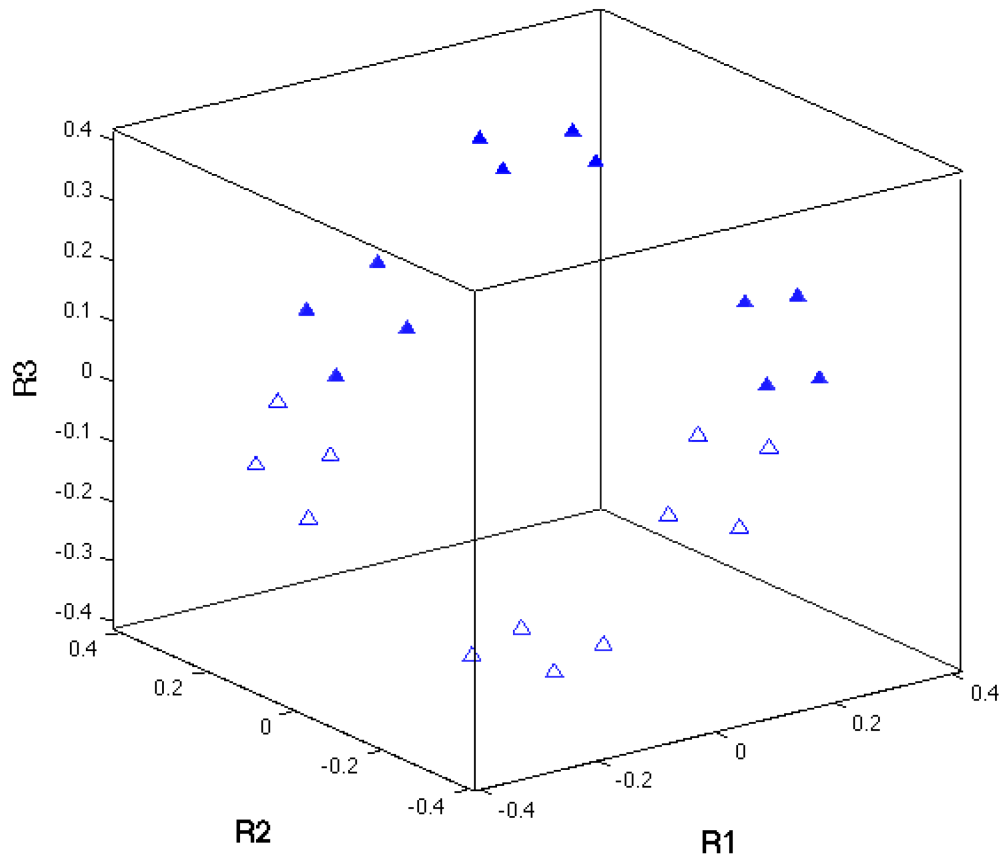


Fig. 9.3. The asymmetric domain for  $(O, O)$  (cubic–cubic) misorientations in Rodrigues space with locations of some CSL misorientations. A rotation representing a CSL is equivalent to its inverse, half of the domain for  $(O, O)$  is sufficient for showing CSL relationships. Such reduction is not allowed if orientation relationships between different phases are considered. The locations of Kurdjumov–Sachs (KS), Nishiyama–Wassermann (NW), Bain (B) and Pitsch (P) orientation relationships are also shown.

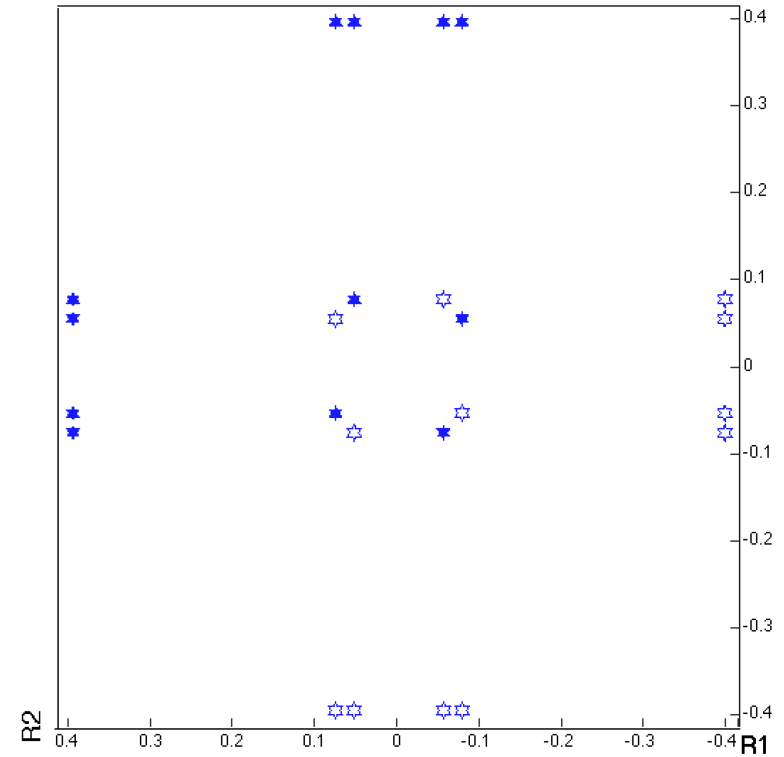
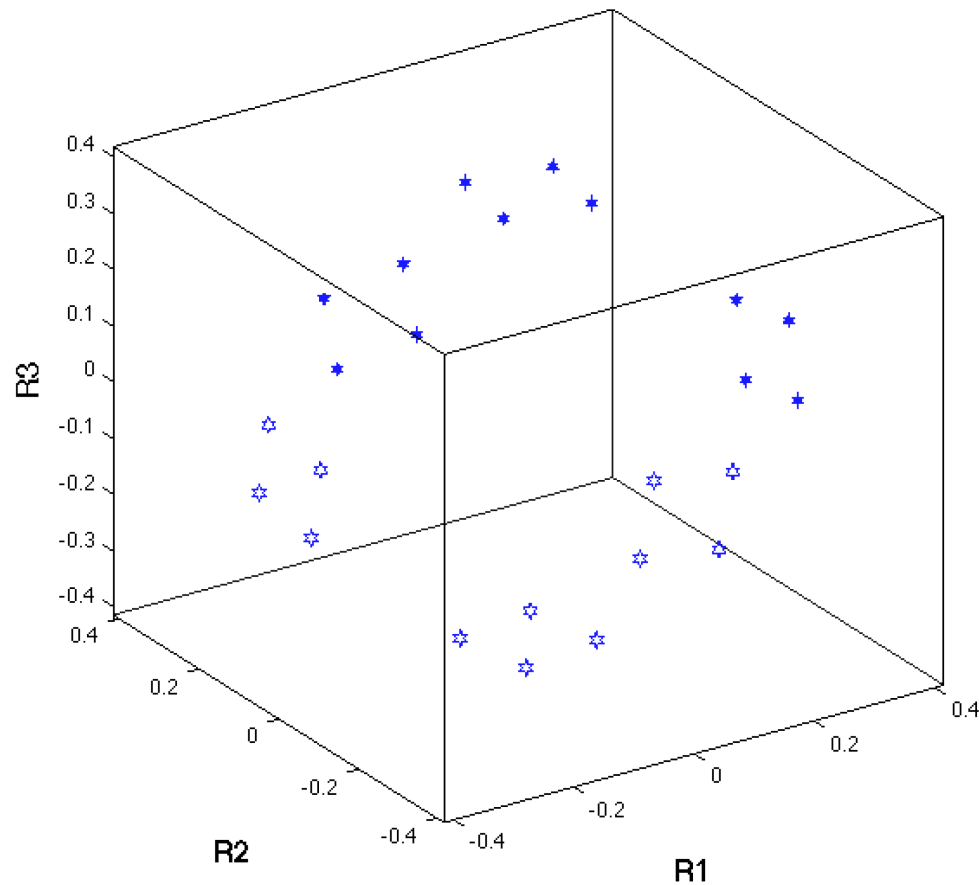
Orientations and Rotations, Adam Morawiec, 2003

# KS Orientation relationship in Rodrigues Space



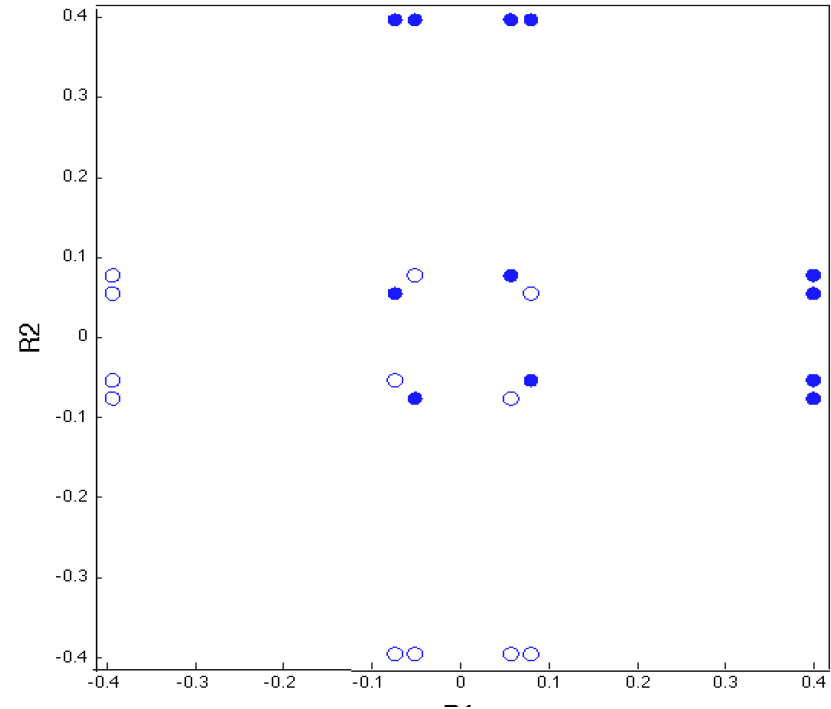
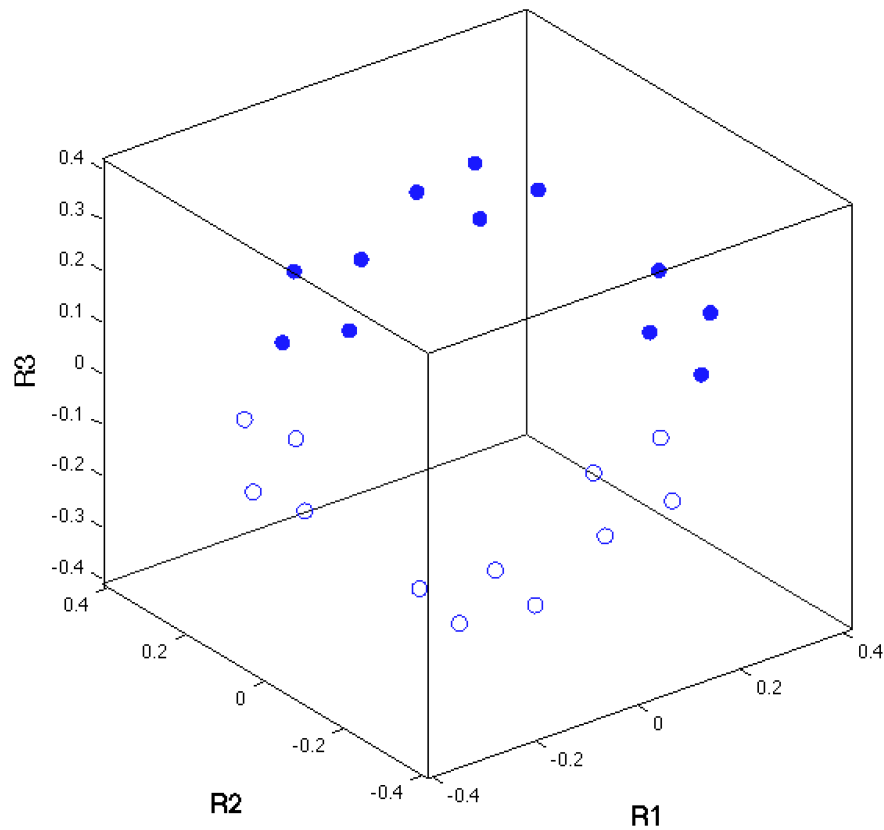
Orientation relationship	Parallelism	Minimum angle/axis	No. of variants
Pitsch (P)	$\{100\}\gamma//\{011\}\alpha$ $\langle 011\rangle\gamma//\langle 111\rangle\alpha$	$45.98^\circ \langle 0.083 \ 0.201 \ 0.976 \rangle$	12
Nishiyama-Wasserman (N-W)	$\{111\}\gamma//\{110\}\alpha$ $\langle 112\rangle\gamma//\langle 110\rangle\alpha$	$45.98^\circ \langle 0.976 \ 0.083 \ 0.201 \rangle$	12
Kurdjumov-Sachs (K-S)	$\{111\}\gamma//\{110\}\alpha$ $\langle 110\rangle\gamma//\langle 111\rangle\alpha$	$42.85^\circ \langle 0.968 \ 0.178 \ 0.178 \rangle$	24
Greninger-Troiano (G-T)	$\{111\}\gamma//\{110\}\alpha$ $\langle 123\rangle\gamma//\langle 133\rangle\alpha$	$44.23^\circ \langle 0.973 \ 0.189 \ 0.133 \rangle$	24
Greninger-Troiano' (G-T')	$\{110\}\gamma//\{111\}\gamma$ $\langle 133\rangle\gamma//\langle 123\rangle\alpha$	$44.23^\circ \langle 0.189 \ 0.973 \ 0.133 \rangle$	24

# GT Orientation relationship in Rodrigues Space



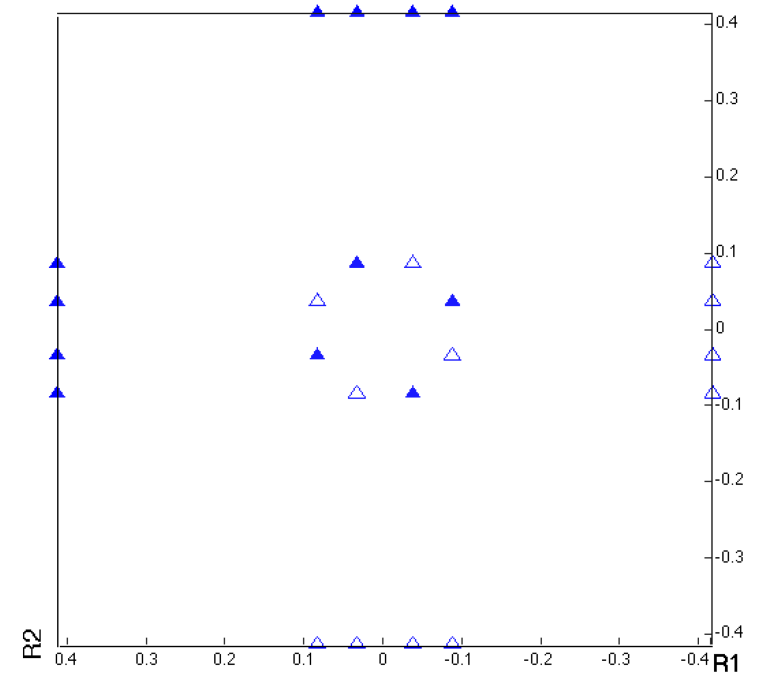
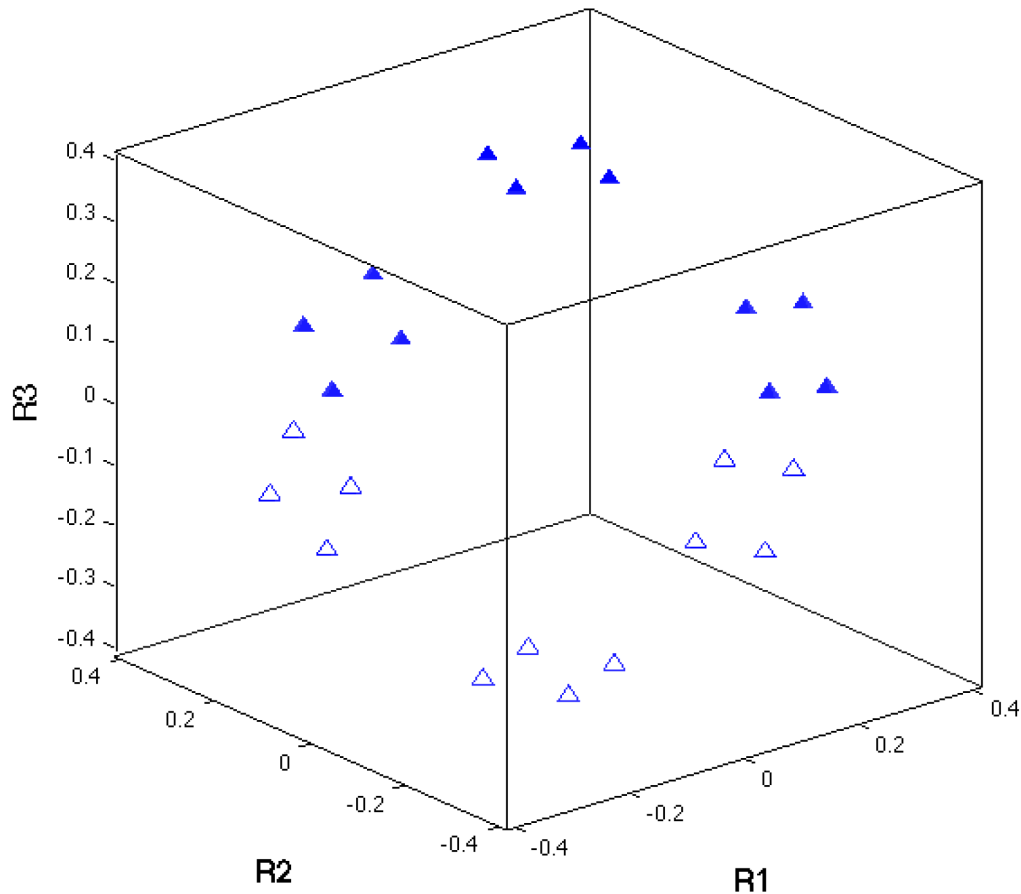
Orientation relationship	Parallelism	Minimum angle/axis	No. of variants
Pitsch (P)	$\{100\}\gamma//\{011\}\alpha$ $\langle 011\rangle\gamma//\langle 111\rangle\alpha$	$45.98^\circ \langle 0.083 \ 0.201 \ 0.976 \rangle$	12
Nishiyama-Wasserman (N-W)	$\{111\}\gamma//\{110\}\alpha$ $\langle 112\rangle\gamma//\langle 110\rangle\alpha$	$45.98^\circ \langle 0.976 \ 0.083 \ 0.201 \rangle$	12
Kurdjumov-Sachs (K-S)	$\{111\}\gamma//\{110\}\alpha$ $\langle 110\rangle\gamma//\langle 111\rangle\alpha$	$42.85^\circ \langle 0.968 \ 0.178 \ 0.178 \rangle$	24
Greninger-Troiano (G-T)	$\{111\}\gamma//\{110\}\alpha$ $\langle 123\rangle\gamma//\langle 133\rangle\alpha$	$44.23^\circ \langle 0.973 \ 0.189 \ 0.133 \rangle$	24
Greninger-Troiano' (G-T')	$\{110\}\gamma//\{111\}\gamma$ $\langle 133\rangle\gamma//\langle 123\rangle\alpha$	$44.23^\circ \langle 0.189 \ 0.973 \ 0.133 \rangle$	24

# GT' Orientation relationship in Rodrigues Space



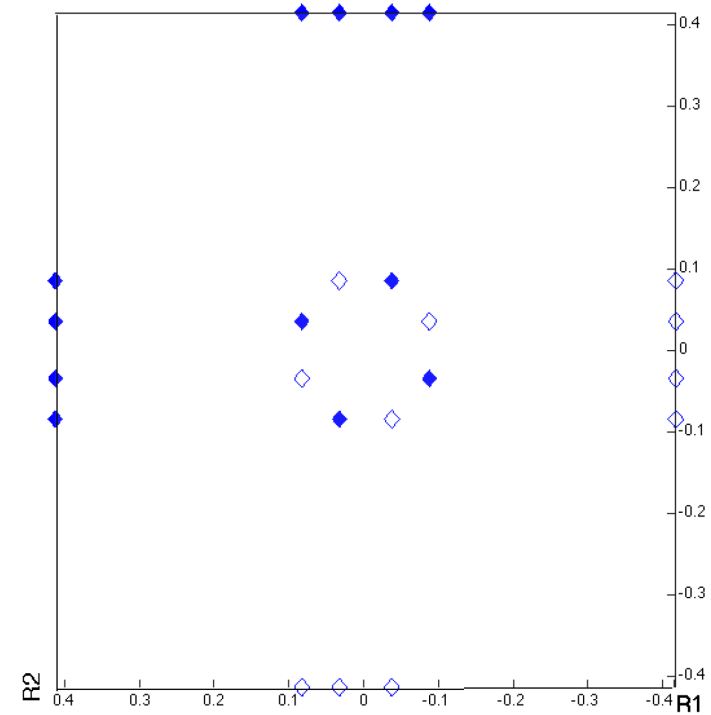
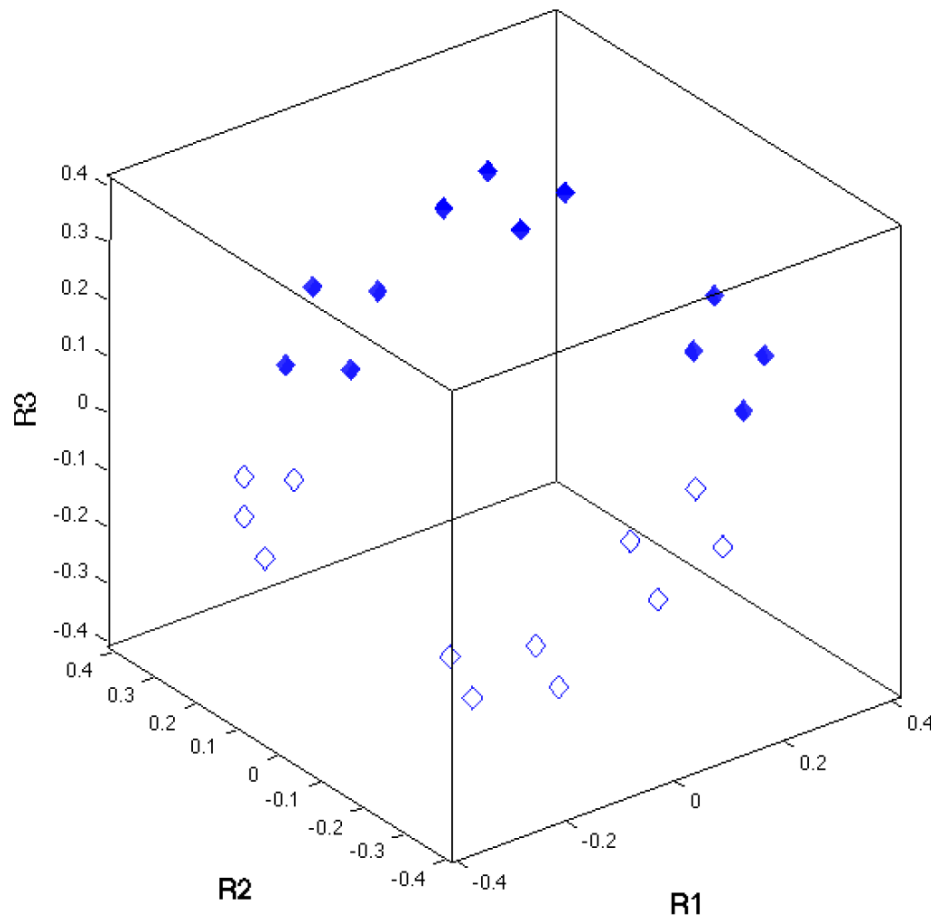
Orientation relationship	Parallelism	Minimum angle/axis	No. of variants
Pitsch (P)	$\{100\}\gamma//\{011\}\alpha$ $\{011\}\gamma//\{111\}\alpha$	$45.98^\circ \langle 0.083 \ 0.201 \ 0.976 \rangle$	12
Nishiyama-Wasserman (N-W)	$\{111\}\gamma//\{110\}\alpha$ $\langle 112 \rangle\gamma//\langle 110 \rangle\alpha$	$45.98^\circ \langle 0.976 \ 0.083 \ 0.201 \rangle$	12
Kurdjumov-Sachs (K-S)	$\{111\}\gamma//\{110\}\alpha$ $\langle 110 \rangle\gamma//\langle 111 \rangle\alpha$	$42.85^\circ \langle 0.968 \ 0.178 \ 0.178 \rangle$	24
Greninger-Troiano (G-T)	$\{111\}\gamma//\{110\}\alpha$ $\langle 123 \rangle\gamma//\langle 133 \rangle\alpha$	$44.23^\circ \langle 0.973 \ 0.189 \ 0.133 \rangle$	24
Greninger-Troiano' (G-T')	$\{110\}\gamma//\{111\}\gamma$ $\langle 133 \rangle\gamma//\langle 123 \rangle\alpha$	$44.23^\circ \langle 0.189 \ 0.973 \ 0.133 \rangle$	24

# NW Orientation relationship in Rodrigues Space



Orientation relationship	Parallelism	Minimum angle/axis	No. of variants
Pitsch (P)	$\{100\}\gamma//\{011\}\alpha$ $\{011\}\gamma//\{111\}\alpha$	$45.98^\circ$ (0.083 0.201 0.976)	12
Nishiyama-Wasserman (N-W)	$\{111\}\gamma//\{110\}\alpha$ $\{112\}\gamma//\{110\}\alpha$	$45.98^\circ$ (0.976 0.083 0.201)	12
Kurdjumov-Sachs (K-S)	$\{111\}\gamma//\{110\}\alpha$ $\{110\}\gamma//\{111\}\alpha$	$42.85^\circ$ (0.968 0.178 0.178)	24
Greninger-Troiano (G-T)	$\{111\}\gamma//\{110\}\alpha$ $\{123\}\gamma//\{133\}\alpha$	$44.23^\circ$ (0.973 0.189 0.133)	24
Greninger-Troiano' (G-T')	$\{110\}\gamma//\{111\}\gamma$ $\{133\}\gamma//\{123\}\alpha$	$44.23^\circ$ (0.189 0.973 0.133)	24

# Pitsch Orientation relationship in Rodrigues Space



Note that the  $\sim 45^\circ$  angle means that the points lie almost on the surfaces of the Rodrigues space for cubic (mis)orientations

Orientation relationship	Parallelism	Minimum angle/axis	No. of variants
Pitsch (P)	$\{100\}\gamma//\{011\}\alpha$ $\{011\}\gamma//\{111\}\alpha$	$45.98^\circ \langle 0.083 \ 0.201 \ 0.976 \rangle$	12
Nishiyama-Wasserman (N-W)	$\{111\}\gamma//\{110\}\alpha$ $\langle 112 \rangle\gamma//\langle 110 \rangle\alpha$	$45.98^\circ \langle 0.976 \ 0.083 \ 0.201 \rangle$	12
Kurdjumov-Sachs (K-S)	$\{111\}\gamma//\{110\}\alpha$ $\langle 110 \rangle\gamma//\langle 111 \rangle\alpha$	$42.85^\circ \langle 0.968 \ 0.178 \ 0.178 \rangle$	24
Greninger-Troiano (G-T)	$\{111\}\gamma//\{110\}\alpha$ $\langle 123 \rangle\gamma//\langle 133 \rangle\alpha$	$44.23^\circ \langle 0.973 \ 0.189 \ 0.133 \rangle$	24
Greninger-Troiano' (G-T')	$\{110\}\gamma//\{111\}\gamma$ $\langle 133 \rangle\gamma//\langle 123 \rangle\alpha$	$44.23^\circ \langle 0.189 \ 0.973 \ 0.133 \rangle$	24



# Forward Texture Prediction

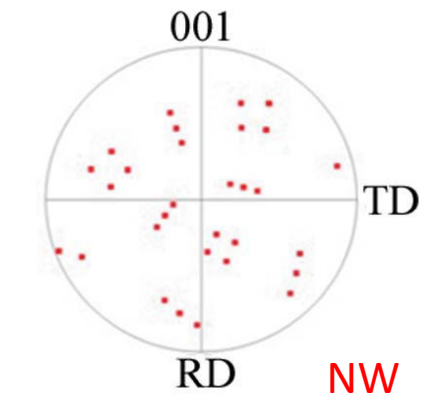
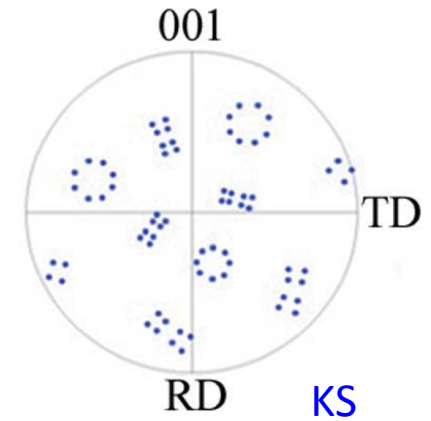
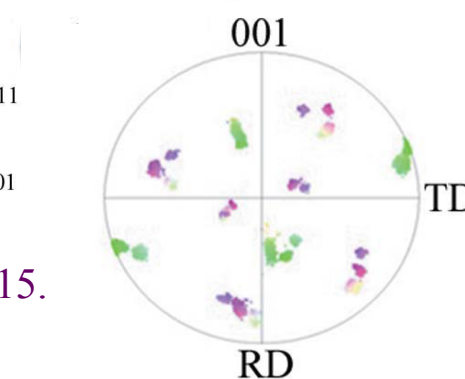
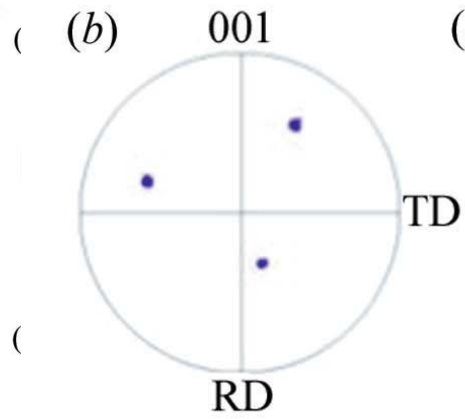
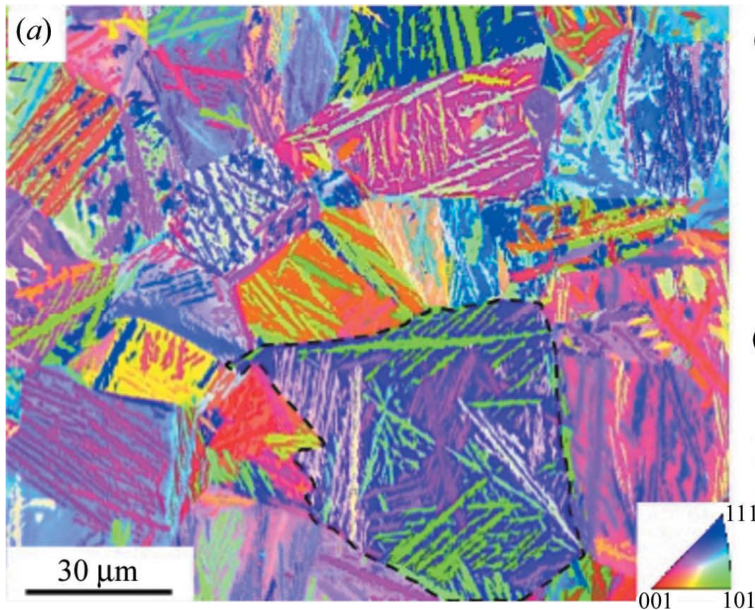
Phase transformation

Parent  
(FCC)



Daughter  
(BCC)

$$g_{ij}^d = T_{ik} \{O_{kp}^c\} g_{pj}^p$$



Tari *et al.* (2013) *J Appl. Cryst.*, **46** 210-215.

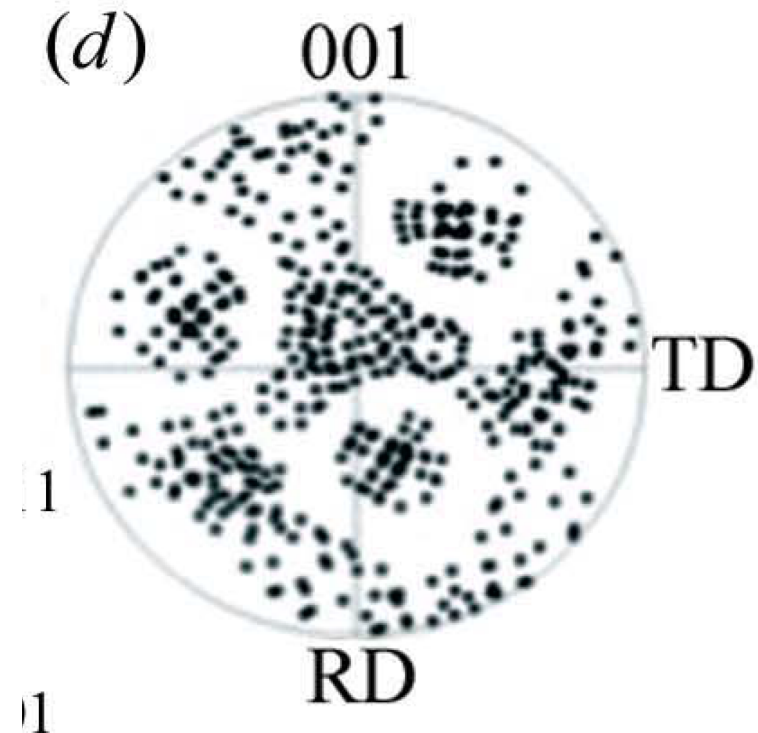
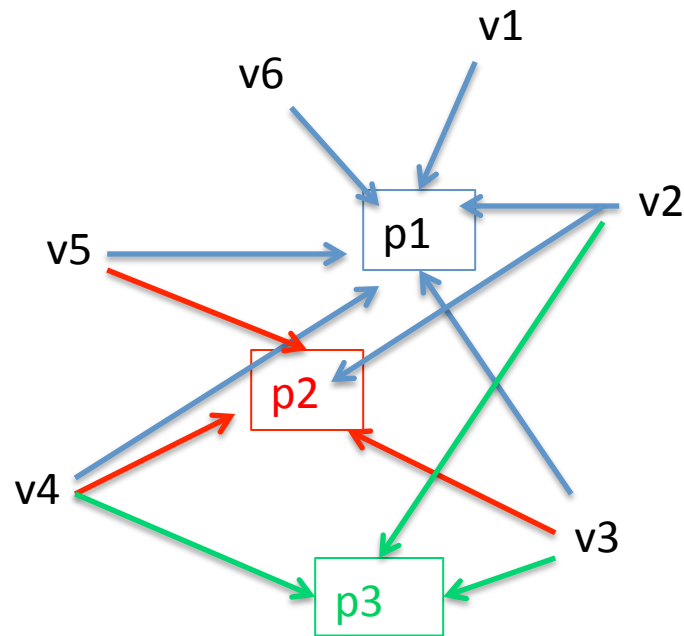
# Backward Texture Calculation

Daughter  
(BCC)

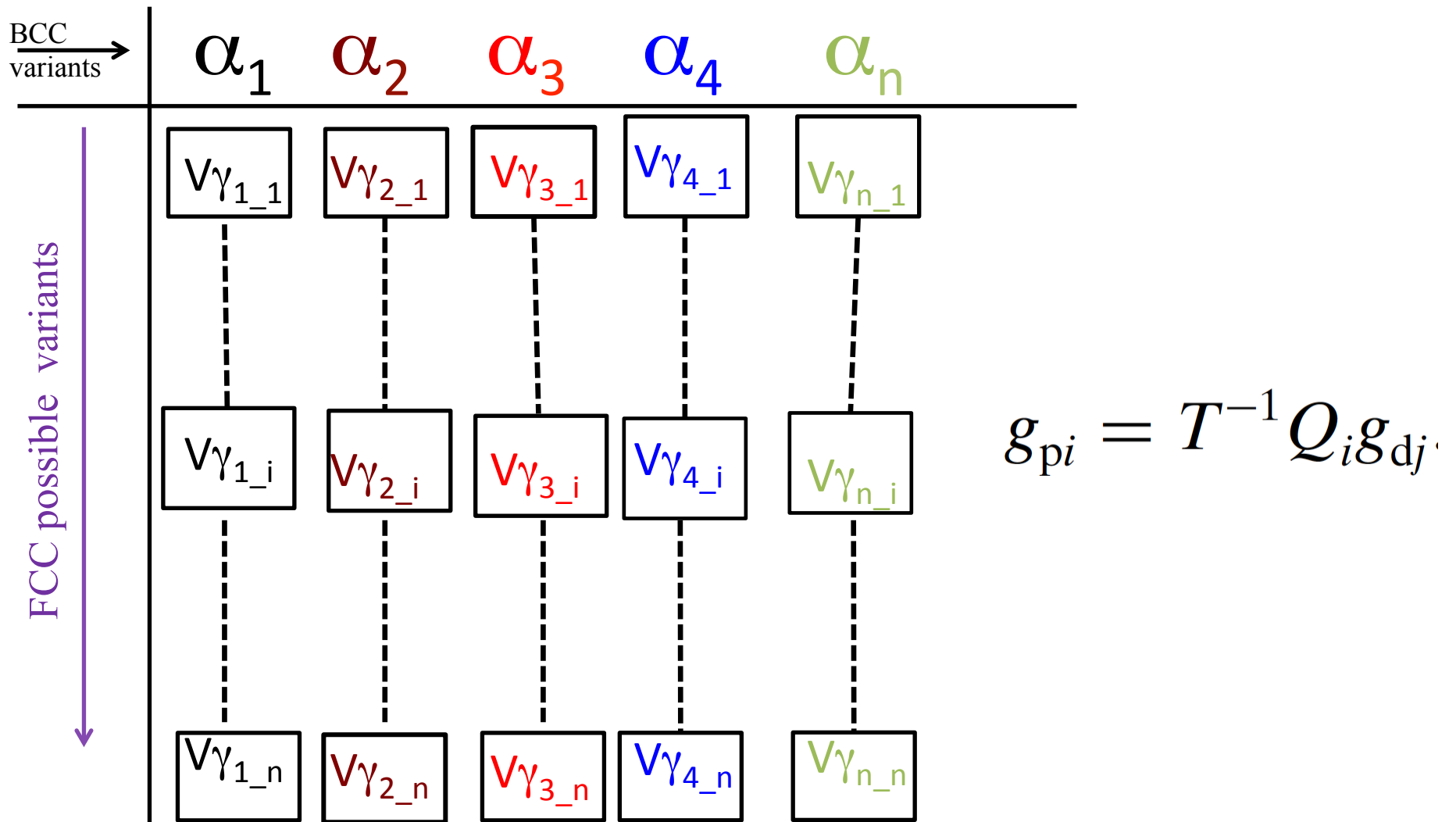


Parent  
(FCC)

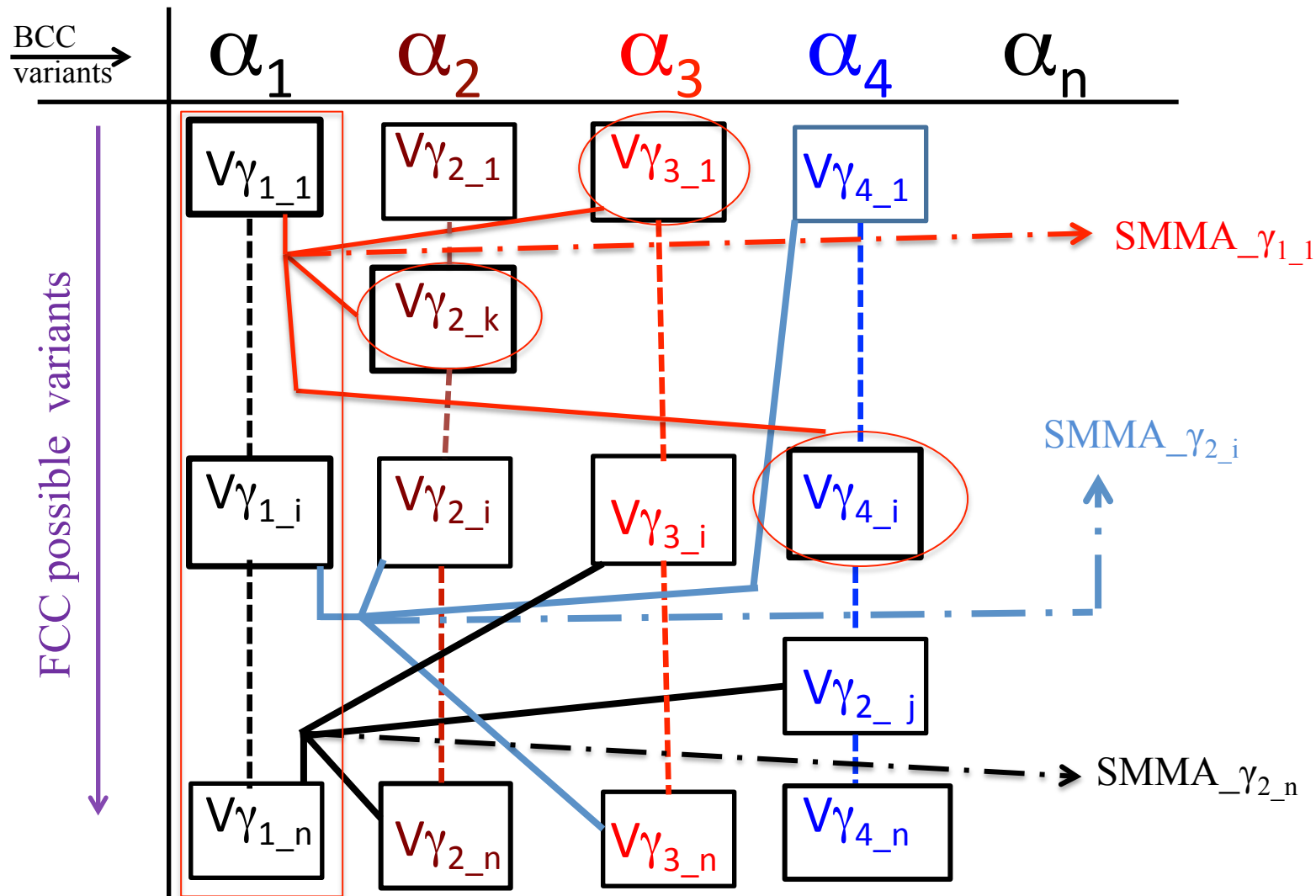
$$g_{pi} = T^{-1} Q_i g_{dj}$$



# Backward Texture prediction

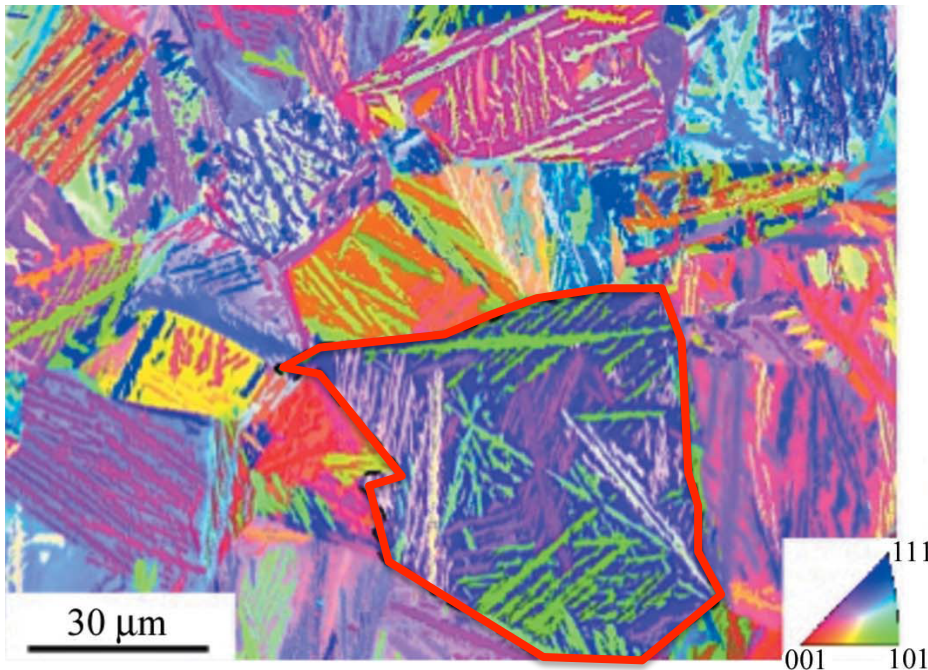


# Backward Texture prediction



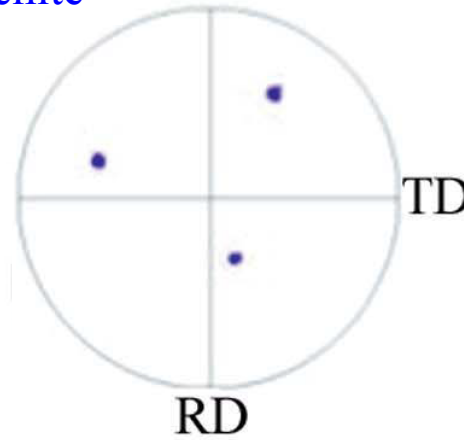
Tari et al. (2013) *J Appl. Cryst.*, **46** 210-215.

# Backward Texture prediction



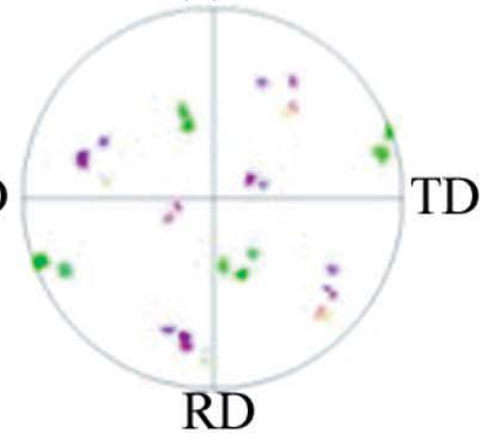
Austenite

001

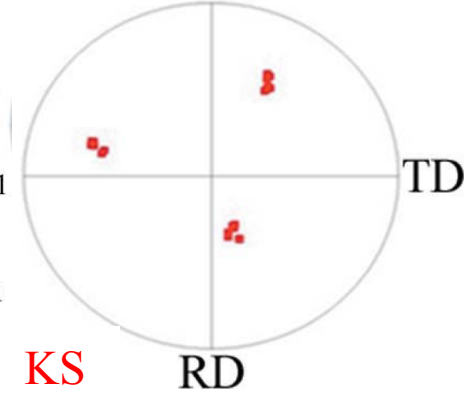


Bainite

001

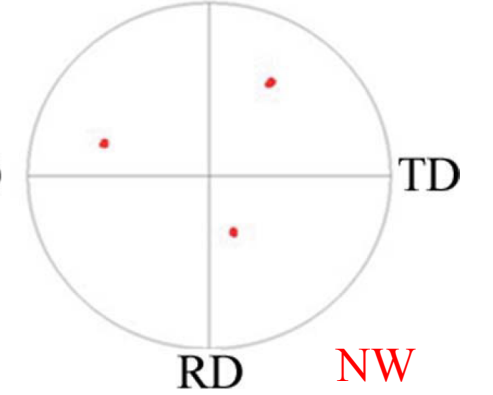


001



KS

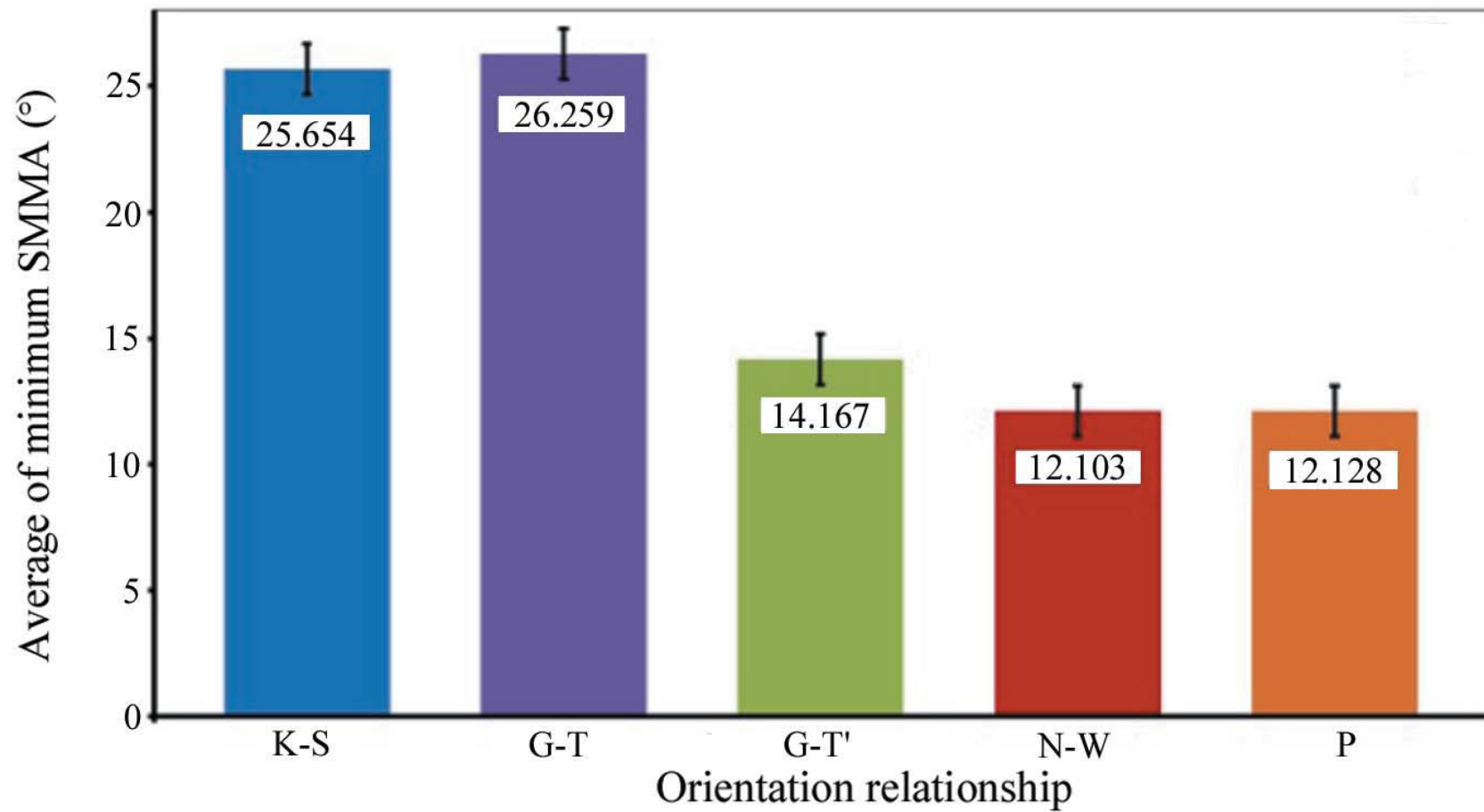
001



NW

$$g_{pi} = T^{-1} Q_i g_{dj}$$

# Backward Texture prediction

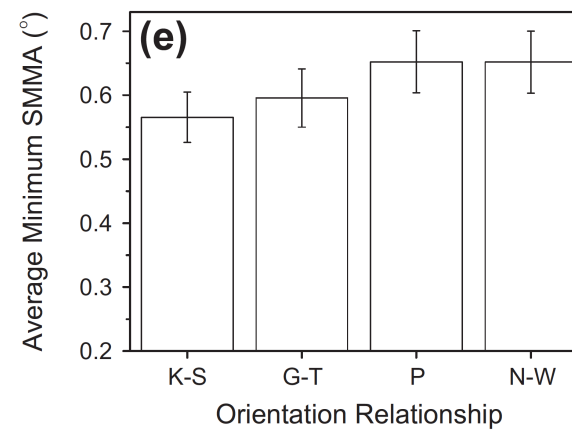
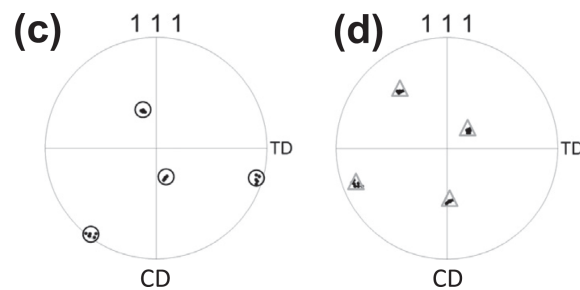
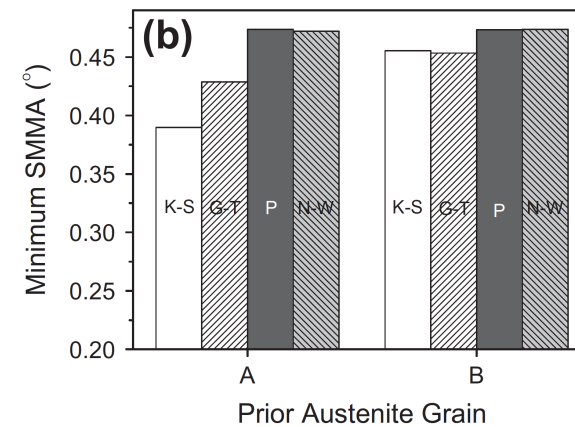
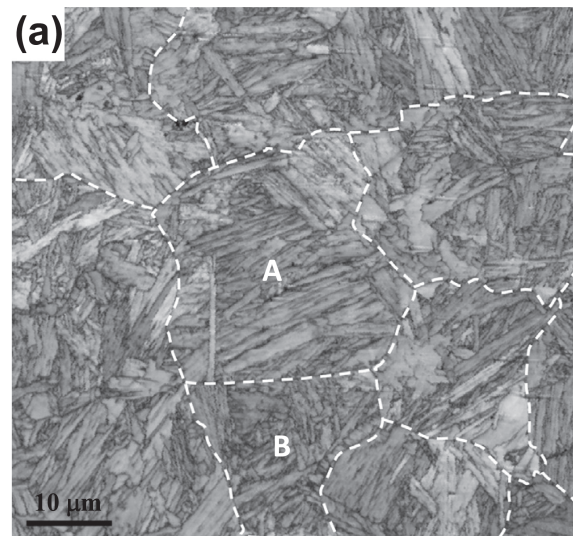


Tari *et al.* (2013) *J Appl. Cryst.*, **46** 210-215.



# Backward Texture prediction

0.04C–1.52Mn–0.2Si–0.22Mo–0.08Ti–0.033Al (in wt.%)



# Orientation Relationships in Pearlite Microstructures

Pearlite is a lamellar structure comprised of BCC  $\alpha$ -ferrite and orthorhombic<sup>1</sup> cementite ( $\text{Fe}_3\text{C}$ ). A schematic of the pearlitic lamellar structure is shown below, with many different length scales represented: prior austenite grain size, pearlite colony size, interlamellar spacing, and cementite thickness. If a high enough microstructural resolution is used, all length scales should be visible in the vpFFT simulations. This may make a case for the use of multiple SVEs rather than RVEs for this microstructure. (Something to be decided later.) Additionally, because of the sharp and (usually) straight ferrite and cementite interface, there likely exists an orientation relationship (OR) between the two phases. In fact, three ORs have been reported in the literature<sup>2</sup>. Two of these ORs occur with a higher frequency than the third, and these two occur with the same frequency. The three ORs are Bagaryatsky<sup>3</sup>, Isaichev<sup>4</sup>, and Pitsch-Petch<sup>5,6</sup> and are described on the lower right. The Isaichev OR is the least frequently observed OR.

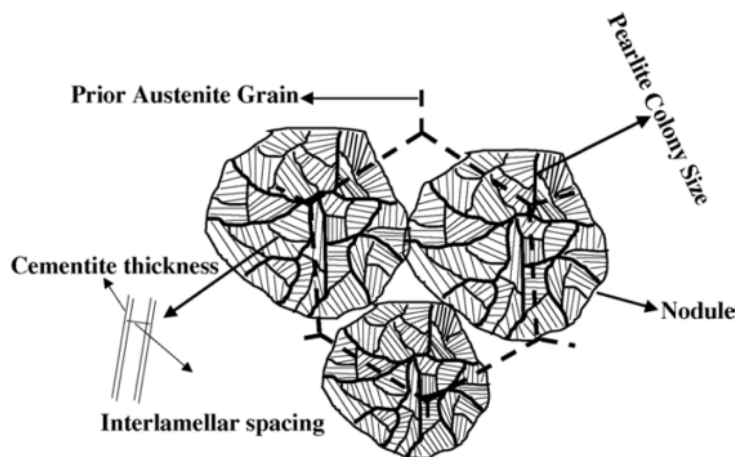


Fig. 1. Schematic diagram illustrating the various constituents in the pearlitic microstructure.

A.M. Elwazri *et al.*,  
Mat Sci and Eng A,  
404 (2005) 91-98

**Bagaryatsky:**

$$\begin{aligned} &[100]_c // [1\bar{1}0]_f \\ &[010]_c // [111]_f \\ &(001)_c // (\bar{1}\bar{1}2)_f \end{aligned}$$

**Isaichev:**

$$\begin{aligned} &[010]_c // \\ &[111]_f \\ &(101)_c // (11\bar{2})_f \end{aligned}$$

**Pitsch-Petch:**

$$\begin{aligned} &[100]_c \text{ 2.6 deg from } [3\bar{1}1]_f \\ &[010]_c \text{ 2.6 deg from } [131]_f \\ &(001)_c // [215]_f \end{aligned}$$

<sup>1</sup>I.G. Wood *et al.*, J Applied Crystallography, 37 (2004) 82-90

<sup>2</sup>M.A. Mangan, G.J. Shiflet, Met Trans A, 30A (1999) 2767-81

<sup>3</sup>Y.A. Bagaryatsky, Dokl Akad Nauk SSSR, 73 (1950)1161-64

<sup>4</sup>I.V. Isaichev, Z Tekhn Fiz, 17 (1947) 835-38

<sup>5</sup>W. Pitsch, Acta Cryst, 10 (1962) 79-80

<sup>6</sup>N.J. Petch, Acta Cryst, 6 (1953) 96



# Further Literature Review of Cementite ORs

Why do different ORs exist for ferrite and cementite in pearlite?

In a large review paper on using electron backscatter diffraction for the study of phase transformations in 2002<sup>1</sup>, a section pertaining to pearlite was presented. It cited a 1999 paper<sup>2</sup> which found that the Pitsch-Petch orientation relationship occurs when the pearlite colony nucleates first with cementite. The Bagaryatsky orientation relationship was observed when the pearlite colony nucleated with ferrite. This was observed in both hypereutectoid or hypoeutectoid alloys. All results of ORs were confirmed using EBSD.

A 2009 review paper<sup>3</sup> on predicting orientation relationships using an edge-to-edge matching method to minimize the misfit at an interface stated that using a “selected area electron diffraction” is insufficient resolution to differentiate between the Isaichev and Bagaryatsky ORs. Higher resolution measurements using convergent beam Kikuchi line diffraction patterns never observed the Bagaryatsky OR. They go as far as to say the Pitsch-Petch OR also does not exist, but it is really four distinct ORs which vary less than 6° from Pitsch-Petch. Additionally, the Bagaryatsky and Isaichev OR vary by about 3.5°.

However, in a 2008 PhD thesis<sup>4</sup> the Bagaryatsky OR was observed using EBSD, which has an angular resolution of about 1-2 degrees.

With the small difference between ORs and EBSD confirmation of the Bagaryatsky, I still believe that the Bagaryatsky OR (along with the Pitsch-Petch OR) is still valid and occur about 50/50.

<sup>1</sup>Gourges-Lorenzen, A.F., *Int. Materials Reviews*, 52 (2002) no. 2

<sup>2</sup>Mangan, Shiflet, *Met Trans A*, 30A (1999) 2767-2781

<sup>3</sup>Zhang, M.X., Kelly, P.M., *Progress in Materials Science*, 54 (2009) 1101-1170

<sup>4</sup>Nikolussi, M., PhD Thesis, 2008

# Pearlite: Hypothesis and Experiments

**Hypothesis:** Pearlite colonies containing the Bagaryatsky OR will deform more than those containing the Pitsch-Petch OR.

---

Concise background relating to hypothesis:

## Orientation Relationships

**Bagaryatsky:**  $[100]_c // [1\bar{1}0]_f$   
 $[010]_c // [111]_f$   
 Habit Planes  $\rightarrow (001)_c // (11\bar{2})_f$

**Pitsch-Petch:**  $[100]_c$  2.6 deg from  $[31\bar{1}]_f$   
 $[010]_c$  2.6 deg from  $[131]_f$   
 Habit Planes  $\rightarrow (001)_c // [215]_f$

## Slip Systems of Pearlite

**Ferrite:**  $\langle 111 \rangle \{110\}$   
 $\langle 111 \rangle \{112\}$

**Cementite:**  $\langle 100 \rangle \{001\}$   
 $\langle 100 \rangle \{011\}$   
 $\langle 111 \rangle \{110\}$

## Isotropic Elevated Yield Stress

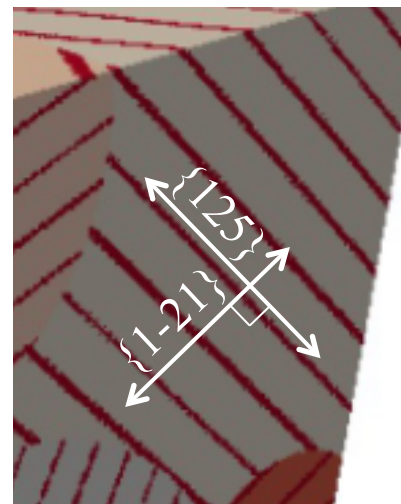
$$\sigma_y = \sigma_0 + k_y S_0^{-1}$$


---



### Bagaryatsky OR

With the slip plane in ferrite aligned to the habit plane, long distance between obstacles on this slip plane

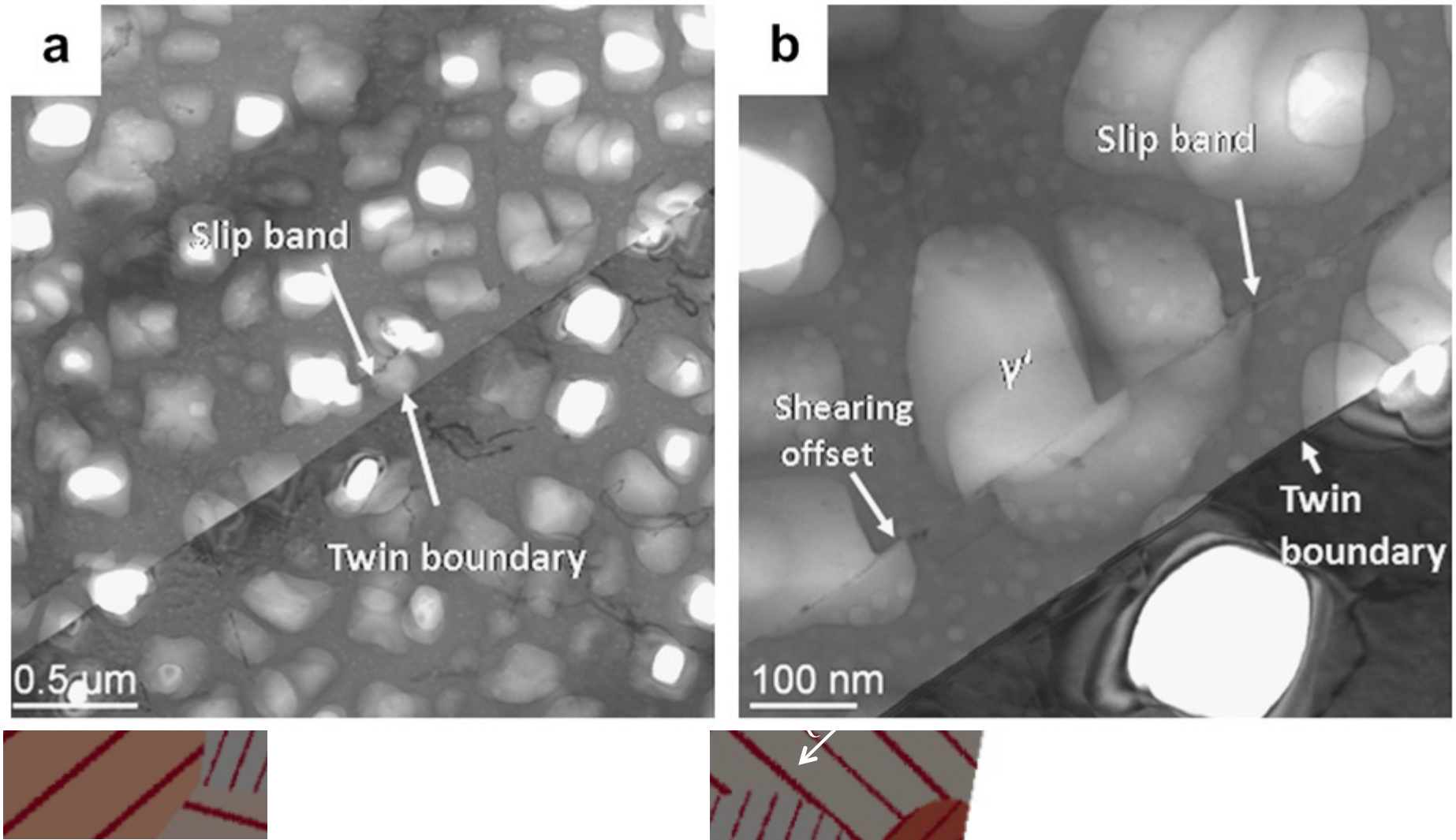


### Pitsch-Petch OR

With the slip plane in ferrite misaligned to the habit plane, short distance between obstacles on the  $\{112\}$  slip planes. In fact,  $\{1-21\}$  is perpendicular to  $\{125\}$

# Pearlite: Hypothesis and Experiments

**Hypothesis:** Pearlite colonies containing the Bagaryatsky OR will deform more than those containing the Pitsch-Petch OR.



# Pearlite: Varying Fractions of the ORs

Testing of this hypothesis is to be performed using the viscoplastic FFT simulations. I am building seven (7) different microstructures from a single parent ferrite grain microstructure. These seven microstructures are:

- 1.) 0\_B-100\_PP – 100% of all parent ferrite grains spawn cementite lamellae with the Pitsch-Petch OR
- 2.) 25\_B-75\_PP – 75% of all parent ferrite grains spawn cementite lamellae with the Pitsch-Petch OR, the other 25% of all parent ferrite grains spawn cementite lamellae with the Bagaryatsky OR
- 3.) 50\_B-50\_PP – 50% of all parent ferrite grains spawn cementite lamellae with the Pitsch-Petch OR, the other 50% of all parent ferrite grains spawn cementite lamellae with the Bagaryatsky OR
- 4.) 75\_B-25\_PP – 25% of all parent ferrite grains spawn cementite lamellae with the Pitsch-Petch OR, the other 75% of all parent ferrite grains spawn cementite lamellae with the Bagaryatsky OR
- 5.) 100\_B-0\_PP – 100% of all parent ferrite grains spawn cementite lamellae with the Bagaryatsky OR
- 6.) Polycrystalline – this microstructure is the parent ferrite grains with a number of ferrite grains switched phase switched to cementite (from ferrite) to match the 16% volume fraction of cementite in pearlite
- 7.) Ferrite only – this microstructure is simply the parent ferrite grains

Recall that there is no true length scale involved in the FFT simulations. So the simulations are not informed as to the length to the nearest boundary which will impede slip on a given slip system. That is to say, these tests will simply test if the introduction of different ORs in the microstructure play a role in the deformation behavior of pearlite. Additionally, comparison of the lamellar microstructure to the polycrystalline sample accentuates the role of the different ORs compared to a simple incorporation of cementite in to the system.

ORs are assigned in the order in which the parent grains are randomly selected making the assignment of OR to each grain random. Additionally, the axis along which the OR is place (the (-1-12) in the case of Bagaryatsky) is also done with a random symmetry operator (belonging to the cubic set).

```

while inserted_twins < desired_number_of_twins AND unfilled_grains?

  Randomly select grainID

  Get grain orientation       $g_i$ 

  while room for twin within grainID

    What is the habit plane normal,  $v_c$ , in crystal reference frame?

    Choose random crystal symmetry operator for crystal class of
      parent grain           $O_c^{(n)}$ 

    Apply crystal symmetry    $v_c' = O_c^{(n)} v_c$ 

    Find direction in sample space    $v_s = g_1^T v_c'$ 

    Construct grain geometry of twin/lamella within parent grain

    Define rotation from parent orientation to twin/lamella
      orientation,  $\Delta g$ , by orientation relationship

    Assign lamella twin/orientation  $g_t$  by
       $g_t = \Delta g O_c^{(n)} g_i$ 

    More twins to insert within grain?

  done

  All grains filled with twins?

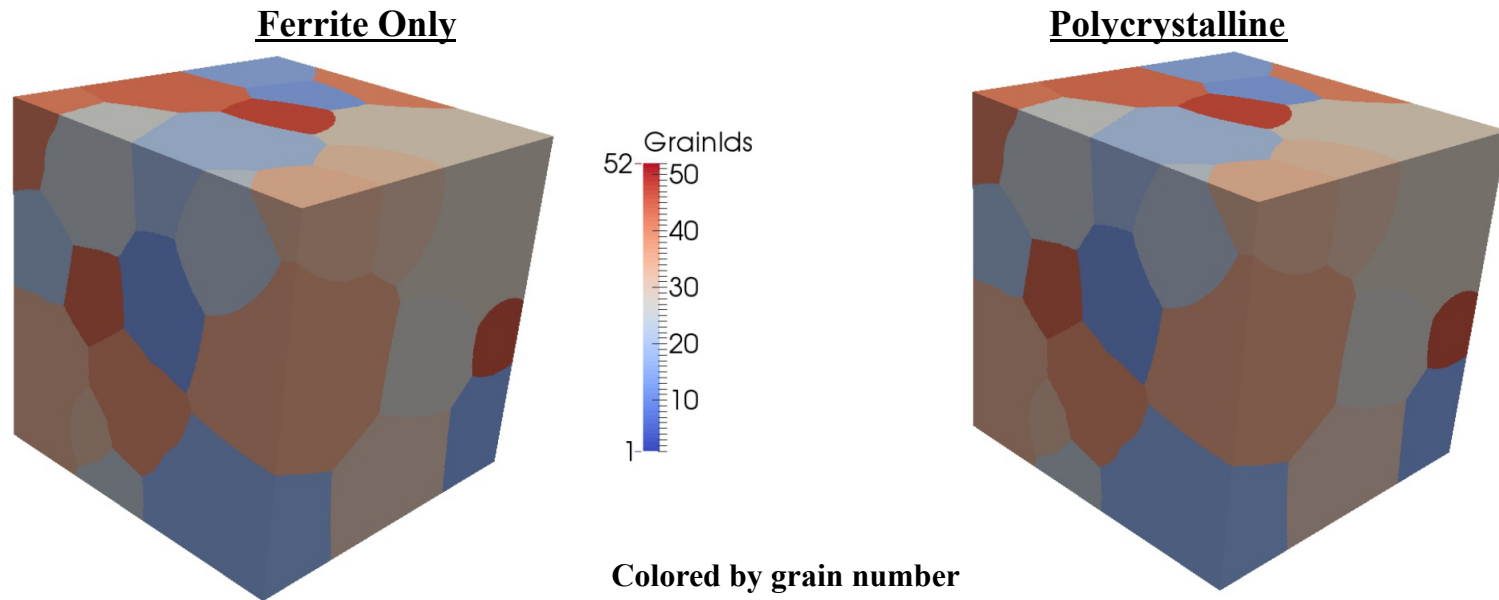
  More twins to insert overall?

done

```

# Pearlite: Varying Fractions of the ORs

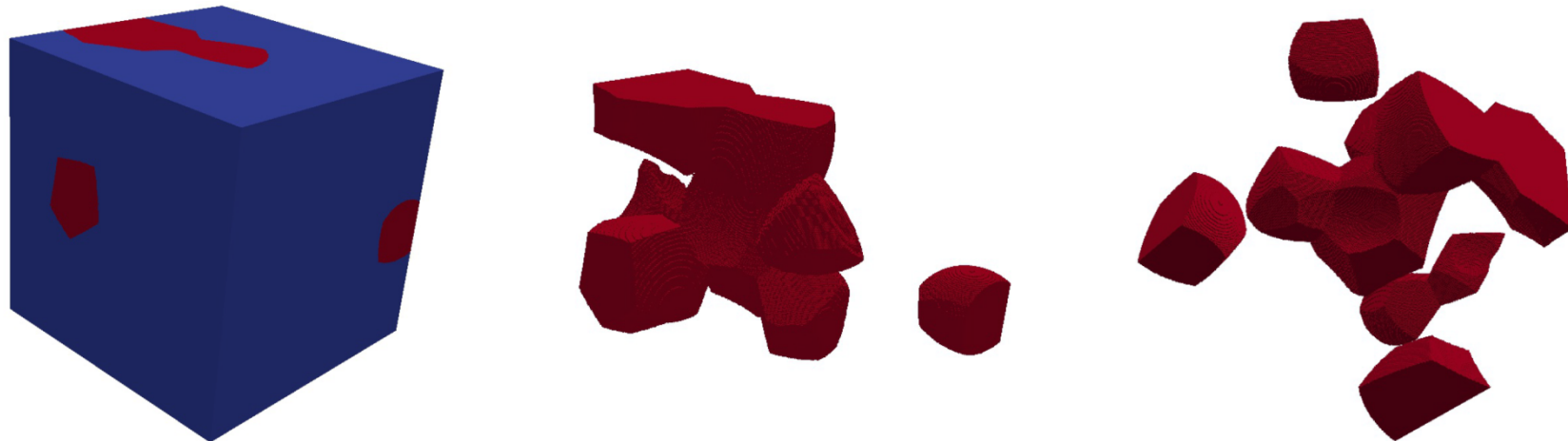
## Grain Structure Images



---

### Polycrystalline – Distribution of Cementite Phase

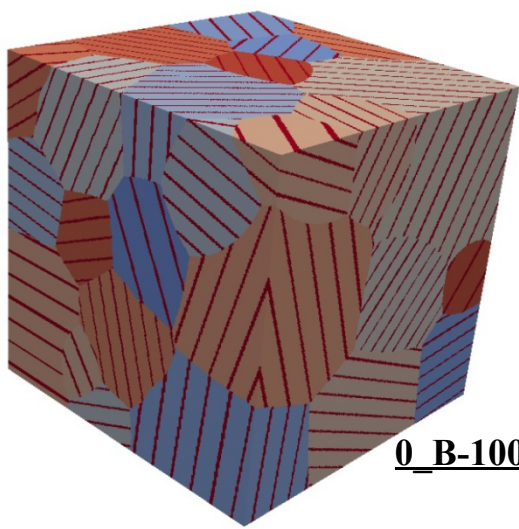
Colored by phase – red = cementite



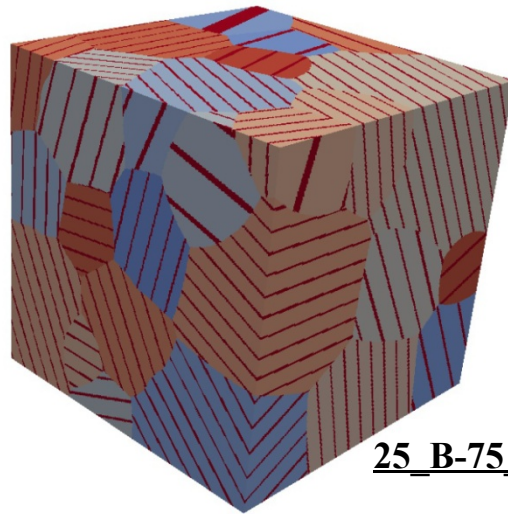


# Pearlite: Varying Fractions of the ORs

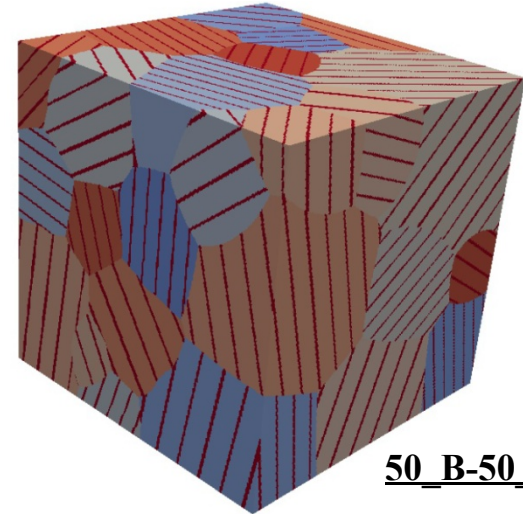
## Grain Structure Images (Cont'd)



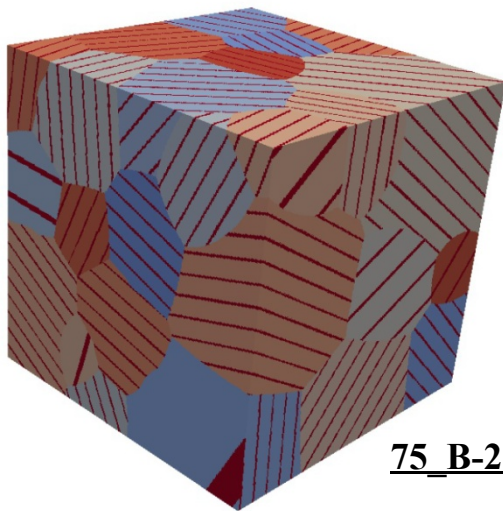
0\_B-100\_PP



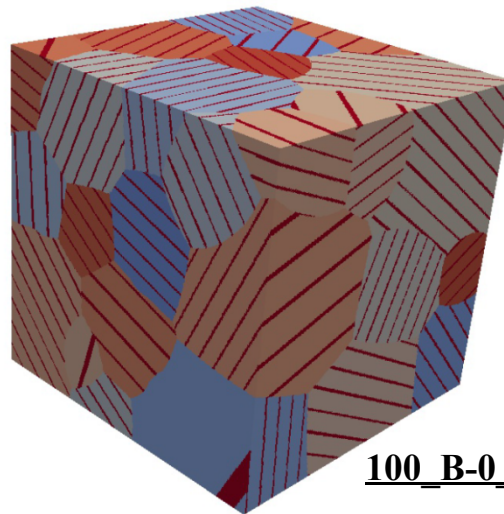
25\_B-75\_PP



50\_B-50\_PP



75\_B-25\_PP



100\_B-0\_PP

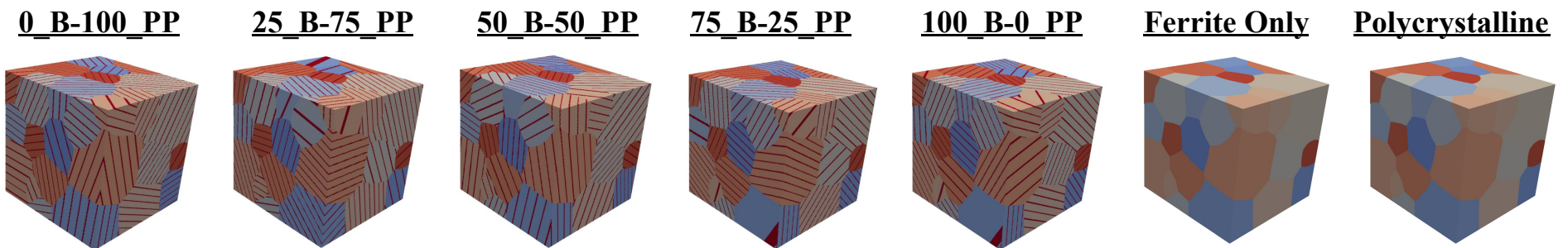
Colored by grain number  
dark red = cementite grains

# Pearlite: Varying Fractions of the ORs Grain Structures

Recall that the Fe-C equilibrium phase diagram predicts the weight fraction of cementite be about 11%. The table on the right displays the measured volume fraction (for simplicity, assumed to be equivalent to weight fraction) of the cementite in each microstructure.

The number of twins inserted in to the 51 parent ferrite grains are also listed.

Structure	Vol. Frac. Cementite	No. of Twins Inserted
0_B-100_PP	0.124	381
25_B-75_PP	0.126	378
50_B-50_PP	0.123	373
75_B-25_PP	0.125	377
100_B-0_PP	0.124	380
Polycrystalline	0.125	0
Ferrite Only	0.000	0
Fe-C Equilibrium Phase Diagram	0.1105	—





# Pearlite: Varying Fractions of the ORs

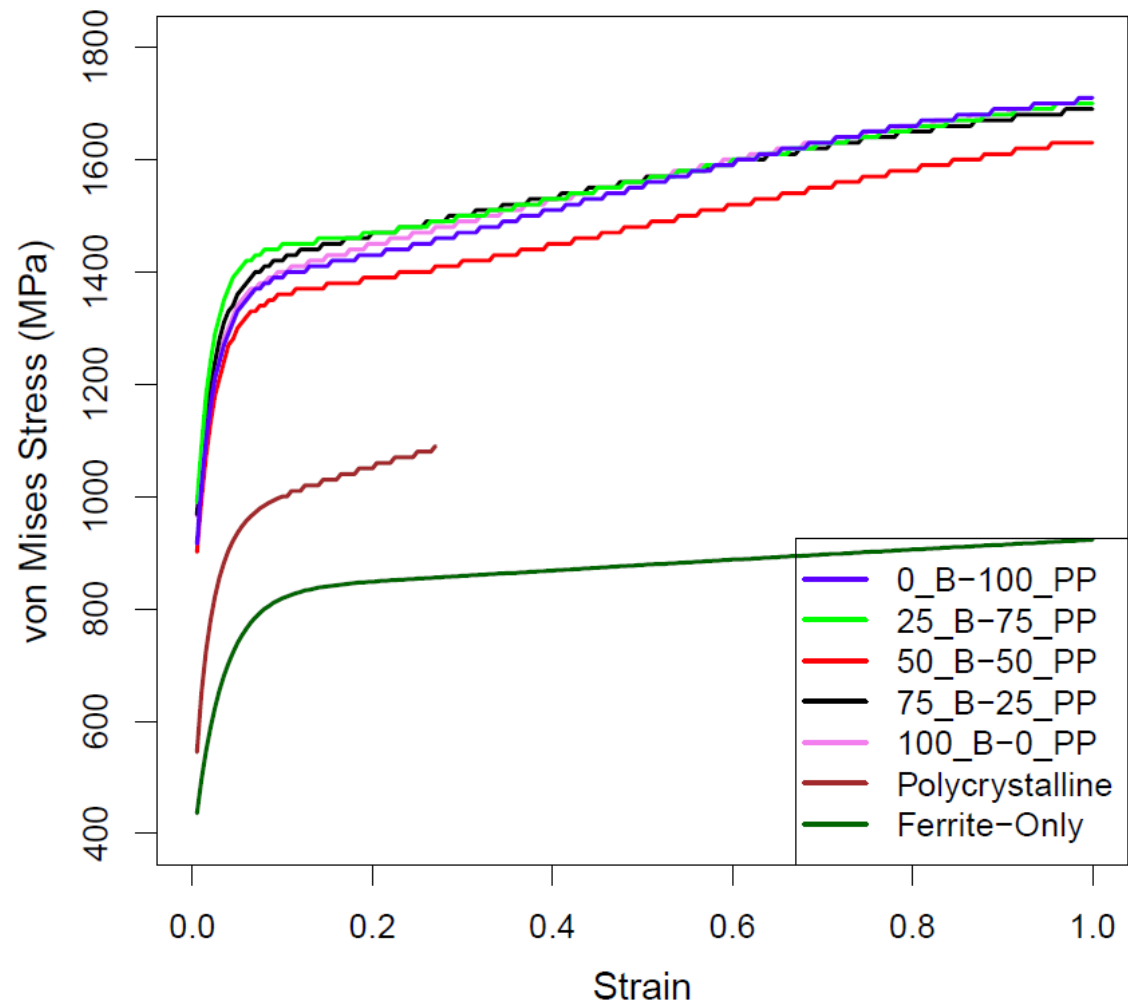
## Stress Strain Curves

These are the overall stress-strain curves for the tested microstructures. The variation in stress response in the pearlitic microstructures no longer increases with increasing Pitsch-Petch orientation relationship.

Notice the lowest stresses are found in microstructures without cementite. Introduction of cementite just as a second phase (polycrystalline) only slightly increases by 200 MPa.

The restriction of cementite to a lamellar structure additionally increases stress values. On average, this is an increase of 350 MPa for the 100\_B-0\_PP microstructure.

The average difference between the 100\_B-0\_PP and 25\_B-75\_PP curves is 80 MPa.



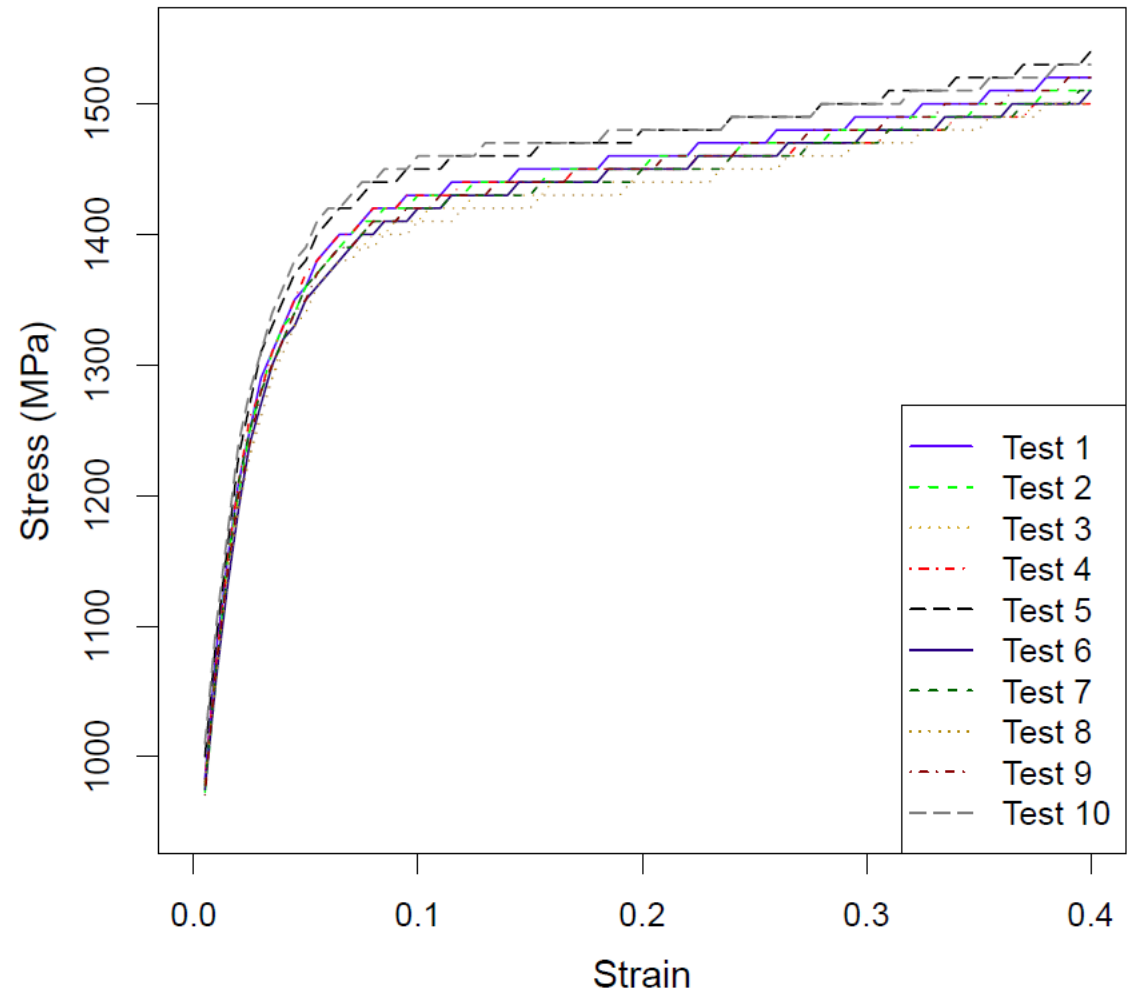
# Pearlite: Varying Fractions of the ORs

## Stress Strain Curves

To test the likelihood of the orientation playing a dominating role on the deformation behavior, I took the original 50\_B-50\_PP grain structure and assigned orientations to all grains at random. I did this 10 times.

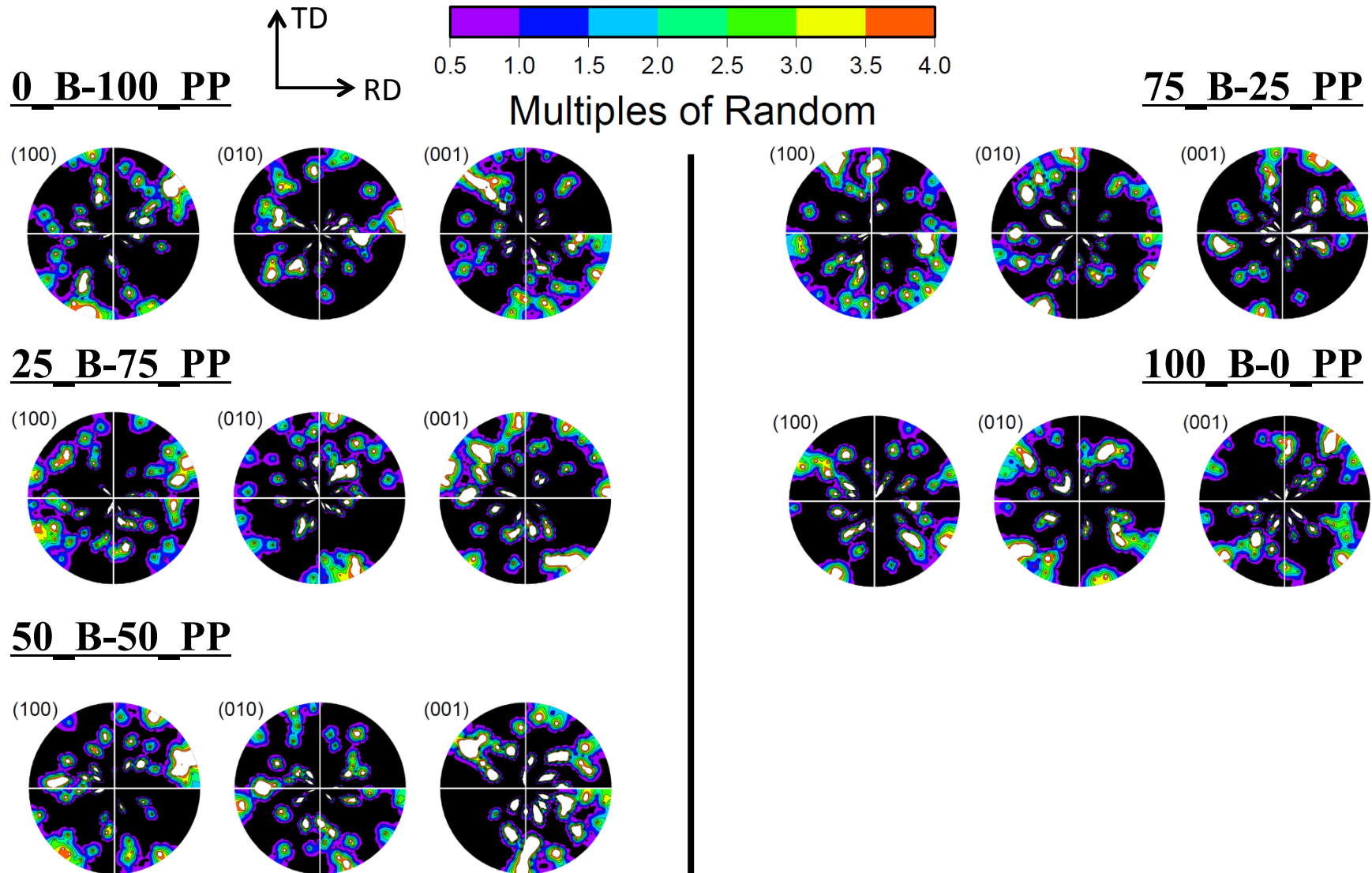
The results to the right show the range of stress response possible for various orientations given this grain structure. The average difference between the highest and lowest stress-strain curves is ~40 MPa.

Therefore, it seems reasonable that some differences in response for the microstructures is due to the structure itself. (i.e. the spatial orientations of the lamellae, which is somewhat controlled by the parent ferrite orientation)

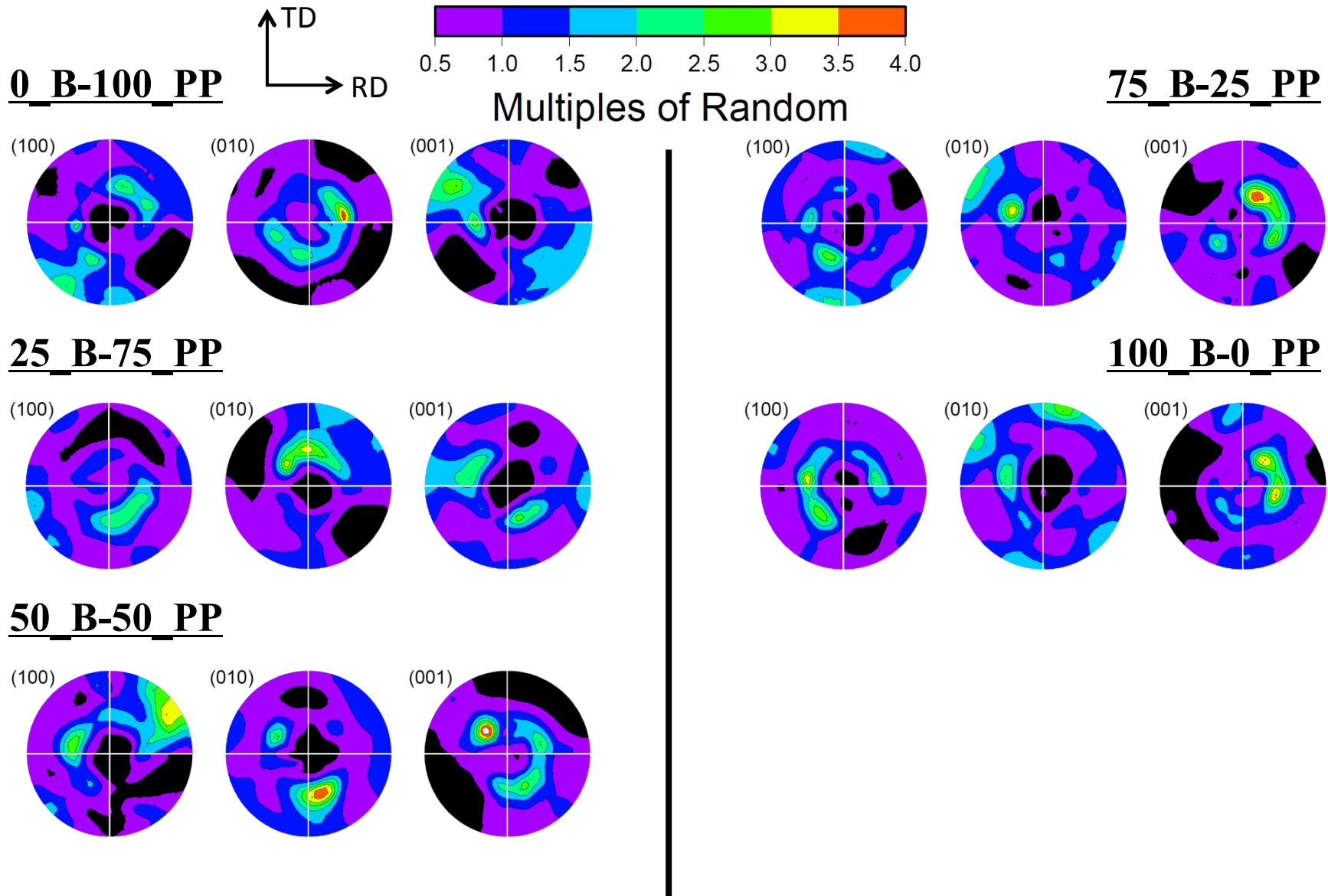


# Texture Development

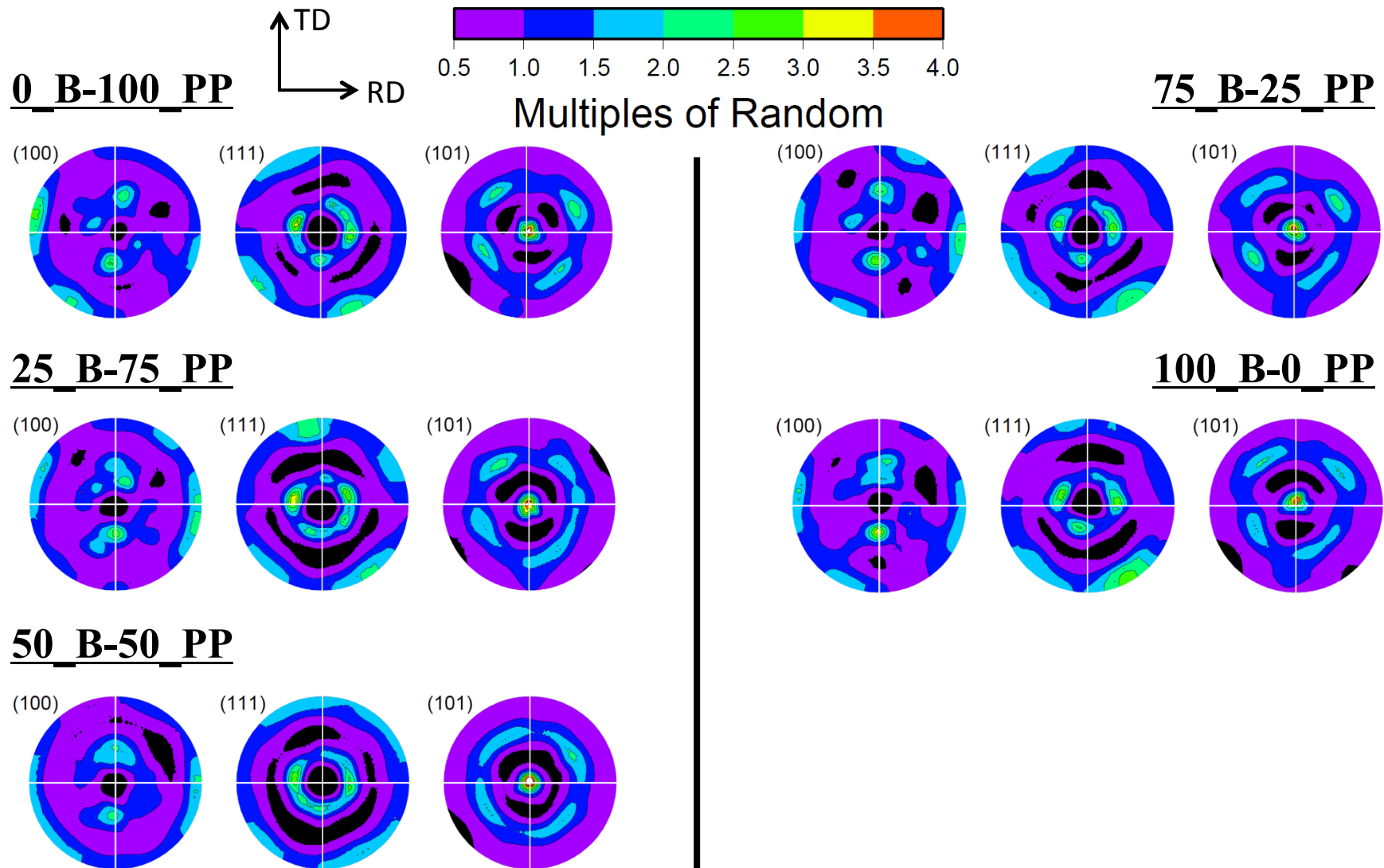
## 0% Strain – Cementite



# Texture Development 100% Strain – Cementite

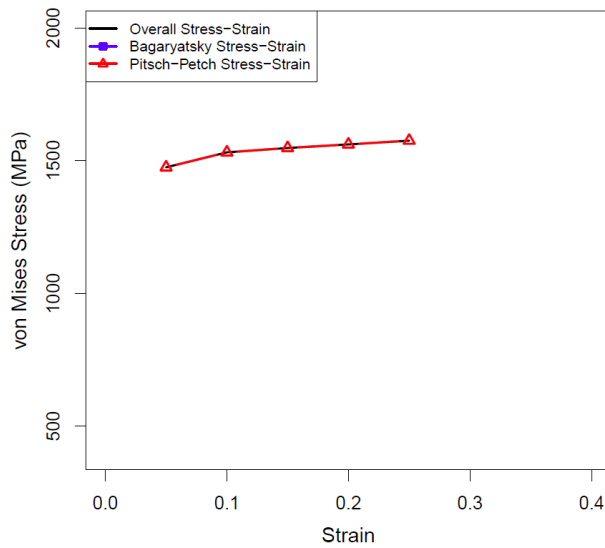


# Texture Development 100% Strain – Ferrite

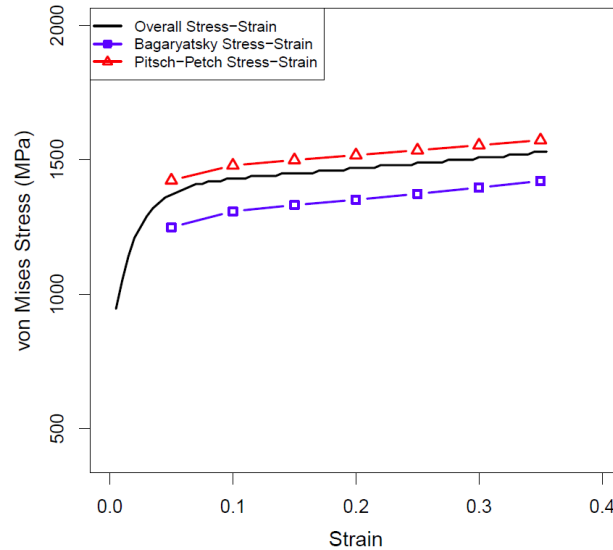


# Partitioning by OR

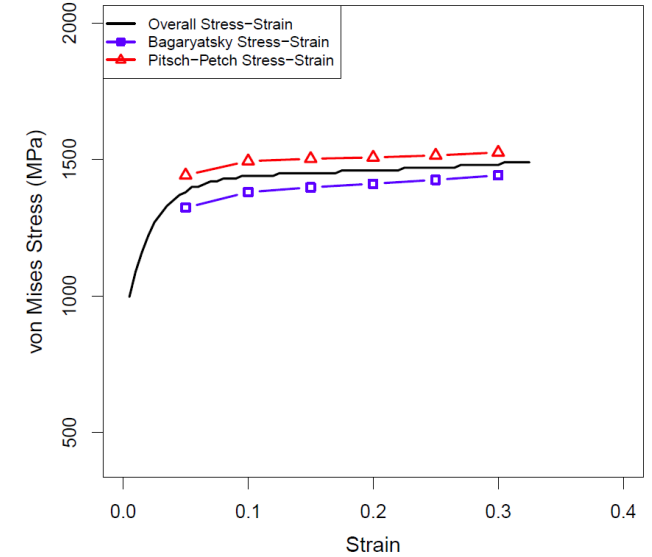
## Non-random ferrite orientations



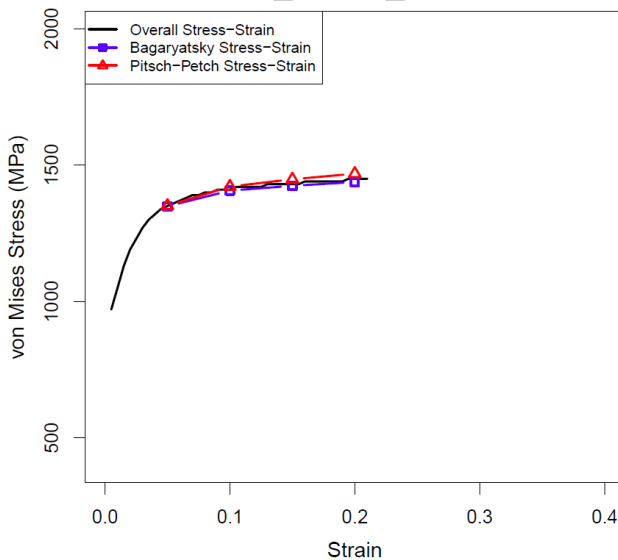
**0\_B-100\_PP**



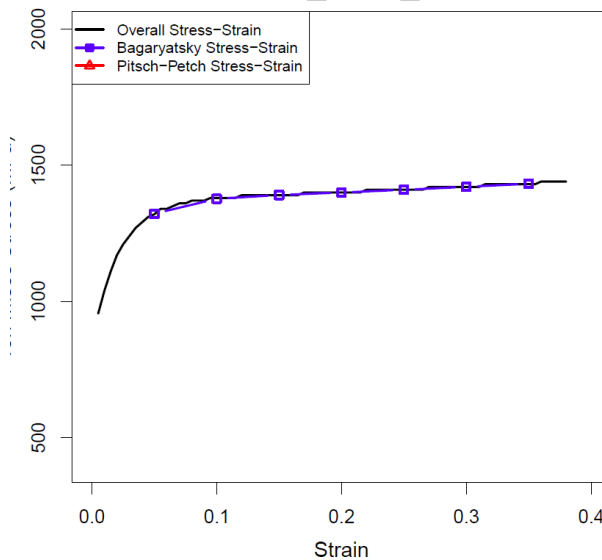
**25\_B-75\_PP**



**50\_B-50\_PP**



**75\_B-25\_PP**



**100\_B-0\_PP**

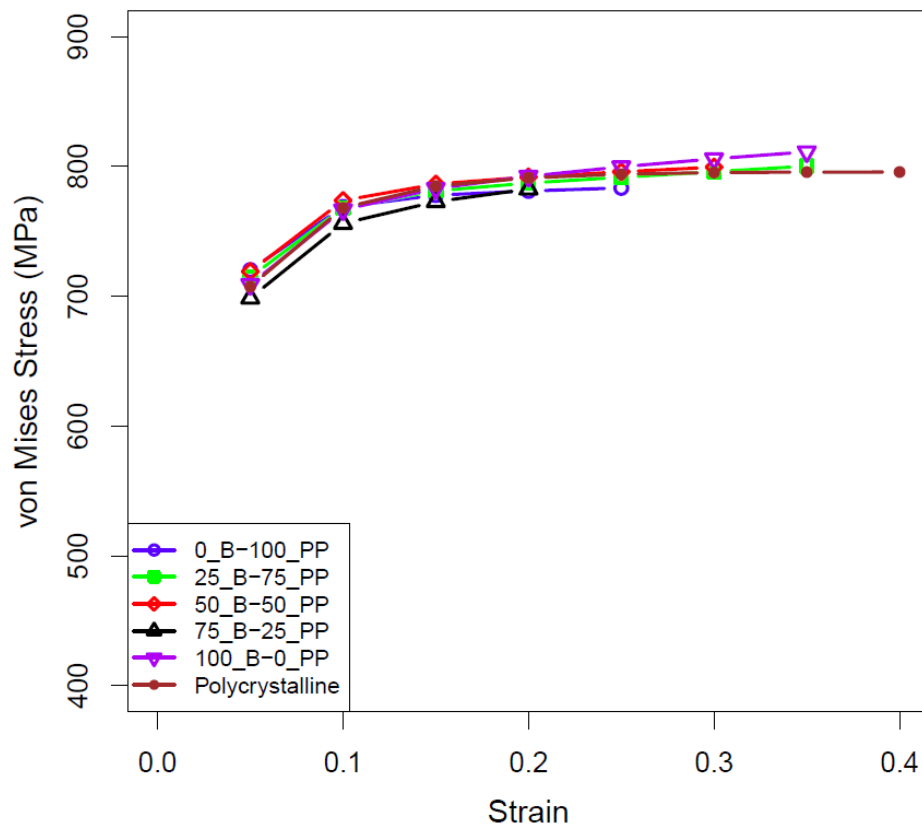
No matter the fraction of the OR present, grains (ferrite and cementite) associated with the Pitsch-Petch OR contain a higher stress value on average than those associated with the Bagaryatsky. This agrees with the hypothesis.

For 0\_B-100\_PP and 100\_B-0\_PP the partitioned values match the overall curve (obviously).

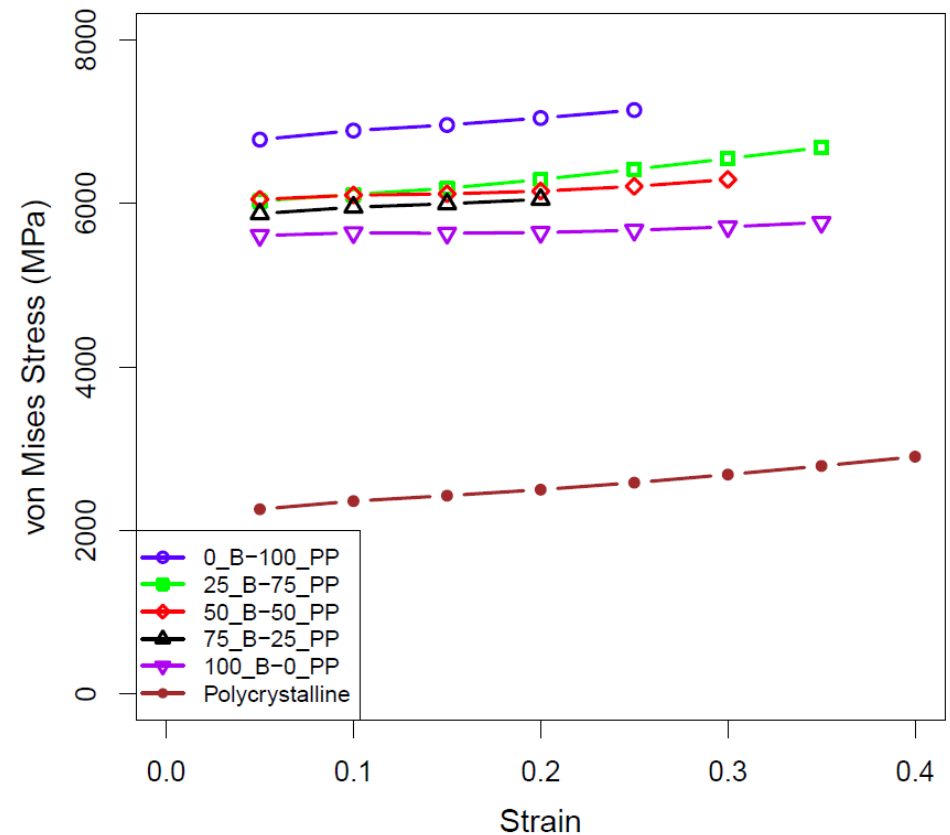
# Partitioning by Phase

## Non-random ferrite orientations

### Ferrite



### Cementite



It is interesting to see that regardless of the OR fraction, the stress values in ferrite do not vary much. However, the cementite stress values seem quite dependent on the OR. While the overall response of the pearlite agrees with the hypothesis, my reasoning seems wrong. I reasoned that in the Bagaryatsky OR the ferrite slip-plane is highly aligned with the interface plane allowing for dislocations to move longer distances prior to encounter obstacles. Currently, I do not have reasoning as to why cementite, instead of ferrite, is sensitive to the OR.

# Microstructure of Martensite

- The microstructural characteristics of martensite are:
  - the product (martensite) phase has a well defined crystallographic relationship with the parent (matrix).
  - martensite forms as platelets within grains.
  - each platelet is accompanied by a shape change
  - the shape change appears to be a simple shear parallel to a habit plane (the common, coherent plane between the phases) and a uniaxial expansion (dilatation) normal to the habit plane. The habit plane in plain-carbon steels is close to  $\{225\}$ , for example (see P&E fig. 6.11).
  - successive sets of platelets form, each generation forming between pairs of the previous set.
  - the transformation rarely goes to completion.



# Microstructures

Martensite formation rarely goes to completion because of the strain associated with the product that leads to back stresses in the parent phase.

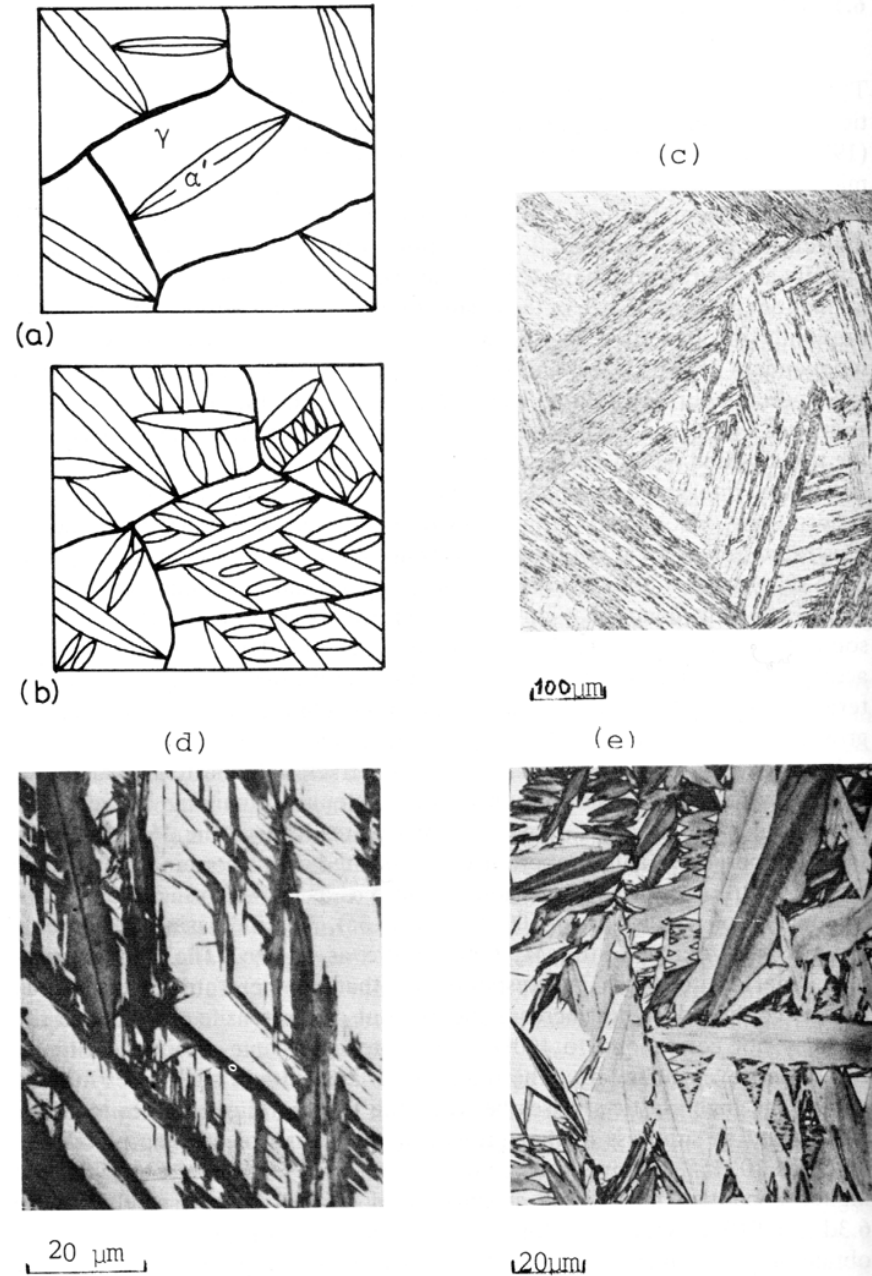


Fig. 6.1 (a), (b) Growth of martensite with increasing cooling below  $M_s$ , (c)–(e) Different martensite morphologies in iron alloys: (c) low C (lath), (d) medium C (plate), (e) Fe–Ni (plate).

# Shear strain in martensite formation

- The change in shape that occurs during martensite formation is important to understanding its morphology.
- In most cases there is a large shear strain. This shear strain is, however, opposed by the surrounding material.
- A typical feature of martensitic transformations is that each colony of martensite laths/plates consists of a stack in which different variants alternate. This allows large shears to be accommodated with minimal macroscopic shear. The reason for this morphology is that the volume of matrix affected by the sheared material is minimized by this alternating pattern of laths.

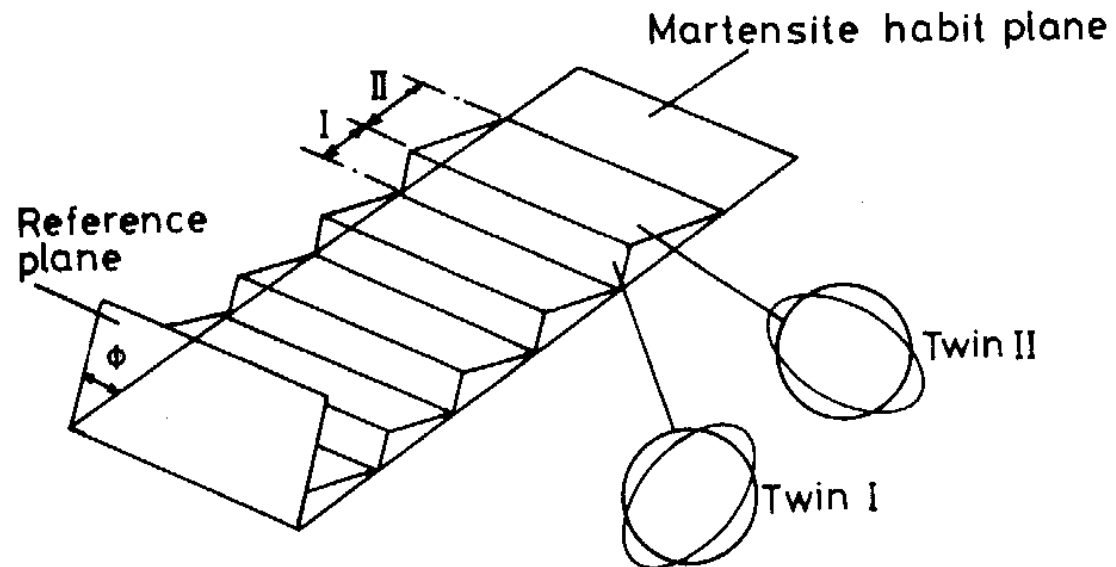
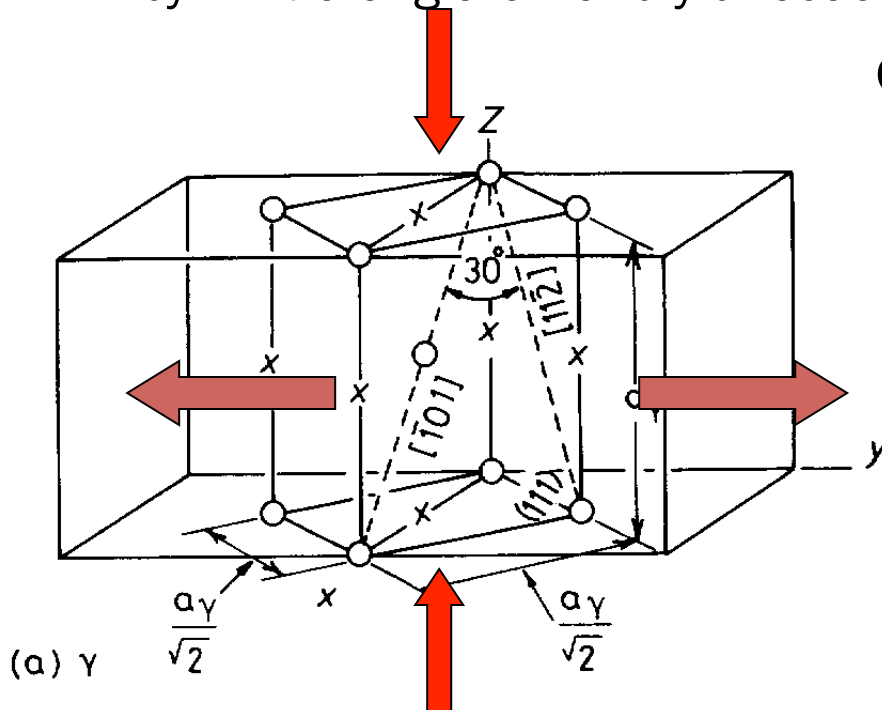


Fig. 6.10 Twins in martensite may be self-accommodating and reduce energy by having alternate regions of the austenite undergo the Bain strain along different axes.

# Atomic model - the Bain Model

- For the case of fcc Fe transforming to body-centered tetragonal (bct) ferrite (Fe-C martensite), there is a basic model known as the Bain model.
- The essential point of the Bain model is that it accounts for the structural transformation with a *minimum of atomic motion*.
- Start with two fcc unit cells: contract by 20% in the z direction, and expand by 12% along the x and y directions.



Orientation relationships in the Bain model are:

$$\begin{aligned} (111)_{\gamma} &\Leftrightarrow (011)_{\alpha'} \\ [101]_{\gamma} &\Leftrightarrow [111]_{\alpha'} \\ [110]_{\gamma} &\Leftrightarrow [100]_{\alpha'} \\ [112]_{\gamma} &\Leftrightarrow [011]_{\alpha'} \end{aligned}$$

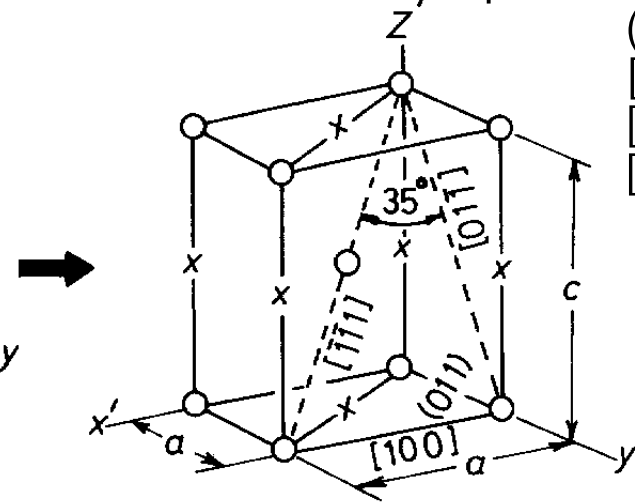


Fig. 6.7 Bain correspondence for the  $\alpha \rightarrow \alpha'$  transformation. Possible interstitial sites for carbon are shown by crosses. To obtain  $\alpha'$  the  $\gamma$  unit cell is contracted about 20% on the C axis and expanded about 12% on the a axes.

*NB The fcc lattice can be obtained from the bcc lattice by expanding in the vertical direction by a factor of  $\sqrt{2}$ .*

# Crystallography, contd.

- Although the Bain model explains several basic aspects of martensite formation, additional features must be added for complete explanations (not discussed in detail here).
- The missing component of the transformation strain is a rotation and an additional twinning shear that changes the character of the strain so as to account for the experimental observation of an *invariant [undistorted] plane*. This is explained in figs. 6.8 and 6.9 and the accompanying text.
- A rather better explanation can be found in *Physical Metallurgy* by P. Haasen, pp 337-343. The best approach to the problem puts it into the form of an *eigenvalue equation*, with transformation matrices to describe each of the 3 component steps of the transformation.

# Role of Dislocations

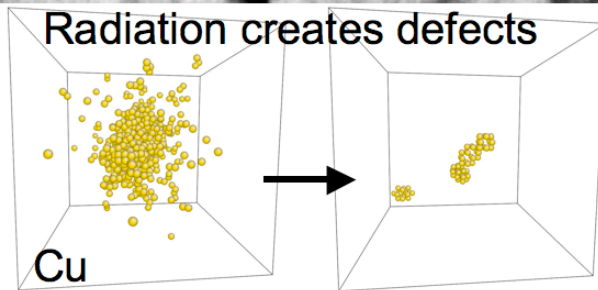
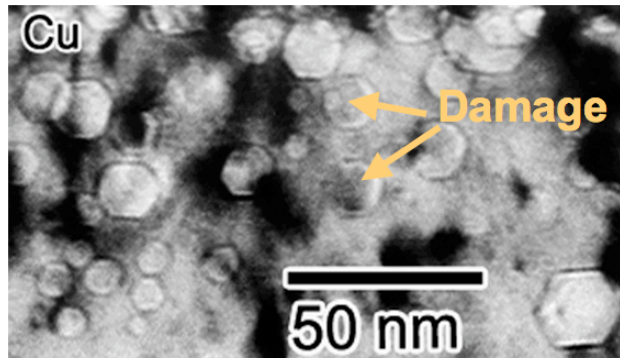
- Dislocations play an important, albeit hard to define role in martensitic transformations.
- Dislocations in the parent phase (austenite) clearly provide sites for heterogeneous nucleation.
- Dislocation mechanisms are thought to be important for propagation/growth of martensite platelets or laths. Unfortunately, the transformation strain (and invariant plane) does not correspond to simple lattice dislocations in the fcc phase. Instead, more complex models of interfacial dislocations are required.

# Cu-Nb laminate composites

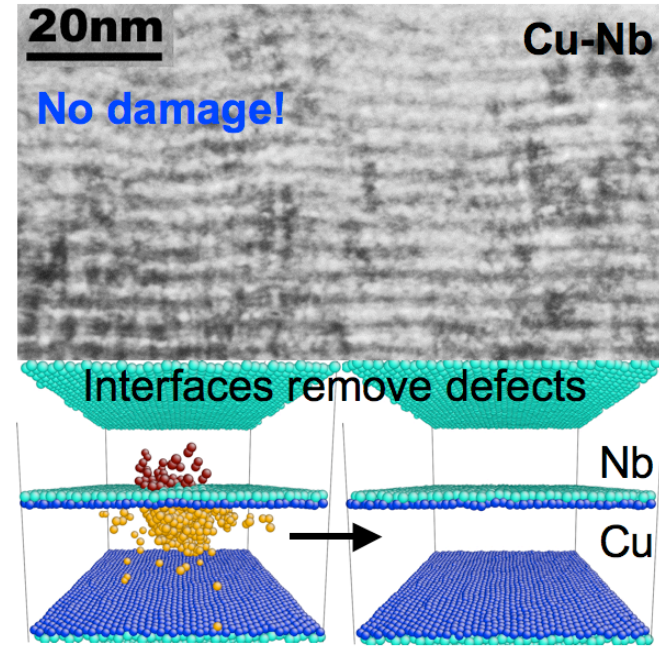
- The next few slides provide information about Cu-Nb composites made by either physical vapor deposition (PVD), or by accumulative roll bonding (ARB). This was the subject of a long-term research program at the Los Alamos National Laboratory.
- Interestingly, the PVD composites exhibited the K-S OR with habit plane being the same as the coincident planes. The ARB composites, however, exhibited the same K-S OR but with variable habit plane.

# Application where OR is important – Accumulated Roll Bonding

Radiation damages bulk crystalline materials



Nanocomposites with high content of certain interfaces are radiation tolerant



After 33keV He<sup>+</sup> bombardment to ~7dpa

- In layered Cu-Nb composites, Kurdjumov-Sachs interface plays an important role, can act as “super sink” to store radiation induced damages, trapping and recombining defects at the interface

- Point defect formation energies are order of magnitude lower and rates of Frenkel pair annihilation significantly higher at interfaces than neighboring crystalline layers
  - Heal damage by trapping and recombining defects before clustering can take place

A. Misra, M. J. Demkowicz, X. Zhang, R. G. Hoagland, JOM **60**, 62 (2007)

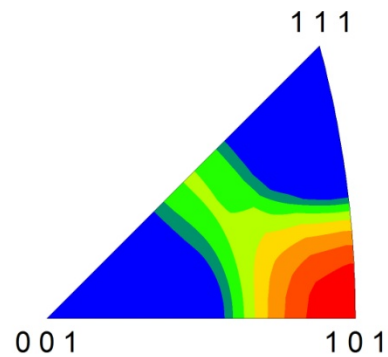
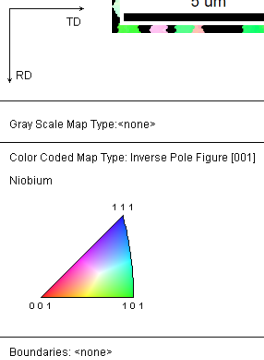
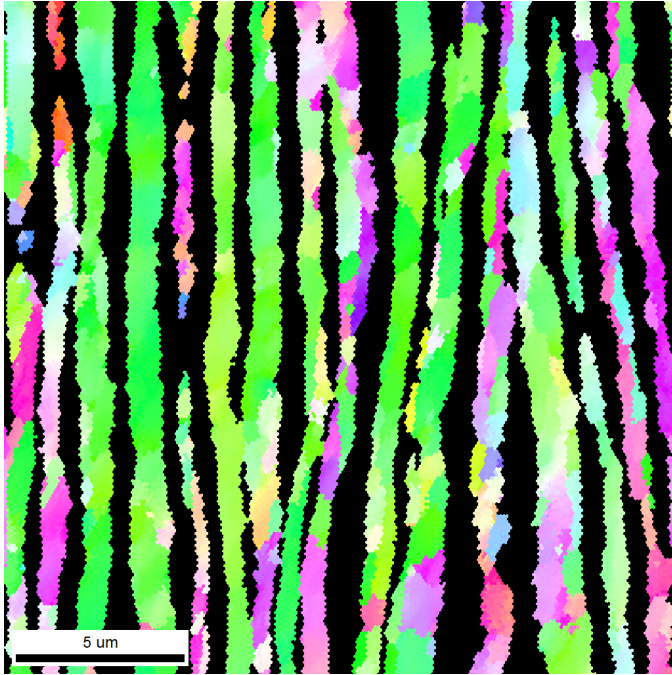


# HIPD Results – ARB

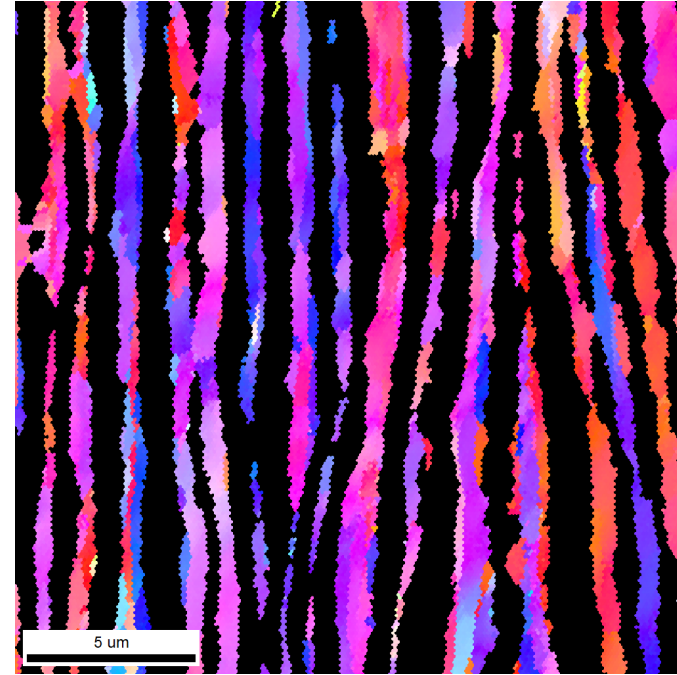
Lee *et al.* (2012) *Acta materialia* 60 1747

HIPD = Heterophase Interphase Plane Distribution

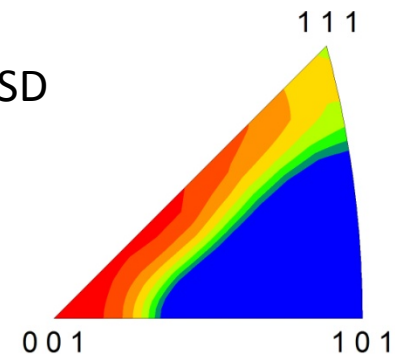
**Cu: FCC**



**Nb: BCC**



770 nm as-rolled, EBSD

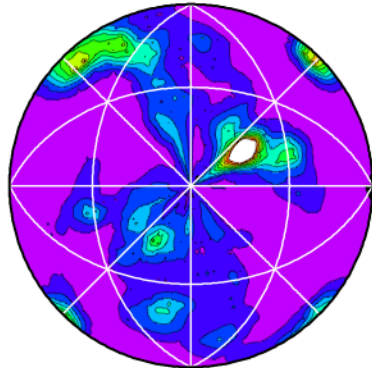


Samples scanned at Los Alamos.

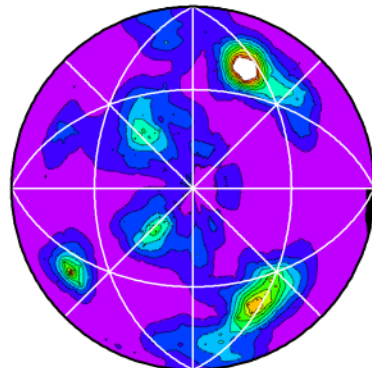


# HICD Results - ARB (KS)

Minimum axis-angle pair,  $42.85^\circ <0.968 \ 0.178 \ 0.178>$



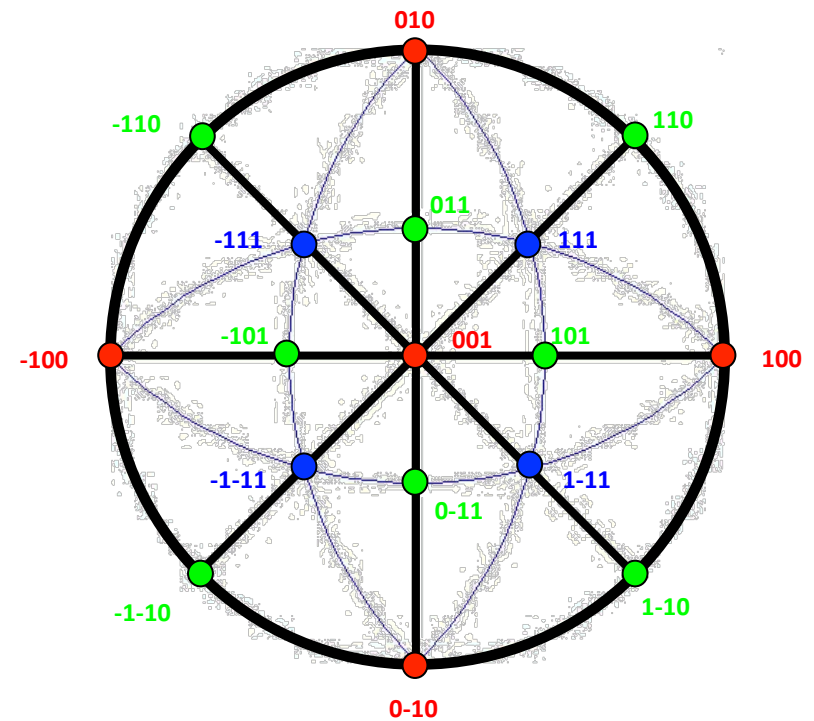
44.88 (max MRD)



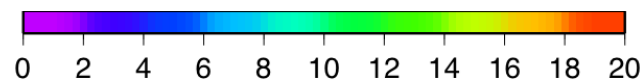
45.68 (max MRD)

*Acta Mater.* **59** (2011) 7744; Demkowicz & Thilly;  $7^\circ$  tilt away from ideal  $\{112\} // \{112\}$  lowers interface energy from 820 down to  $690 \text{ mJ/m}^2$

**001 standard stereographic projection**



770 nm as-rolled, EBSD



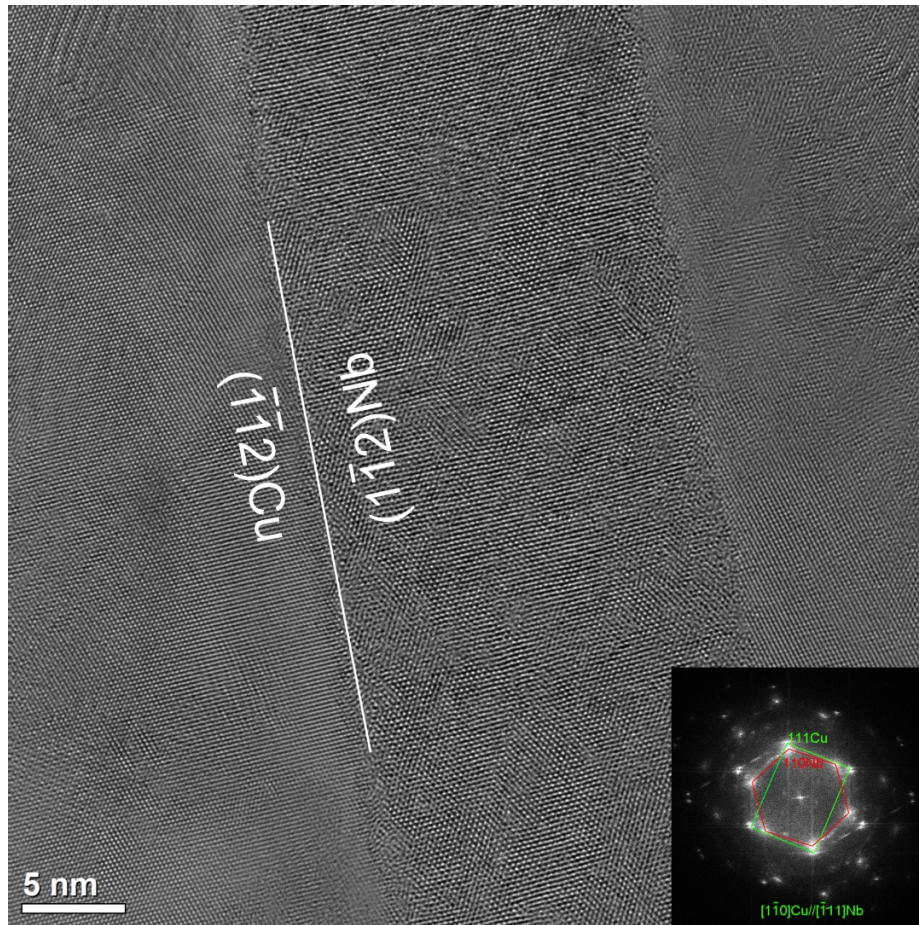
Multiples of Random

# Ex Situ Thermal stability Study of ARB Cu-Nb (18nm)

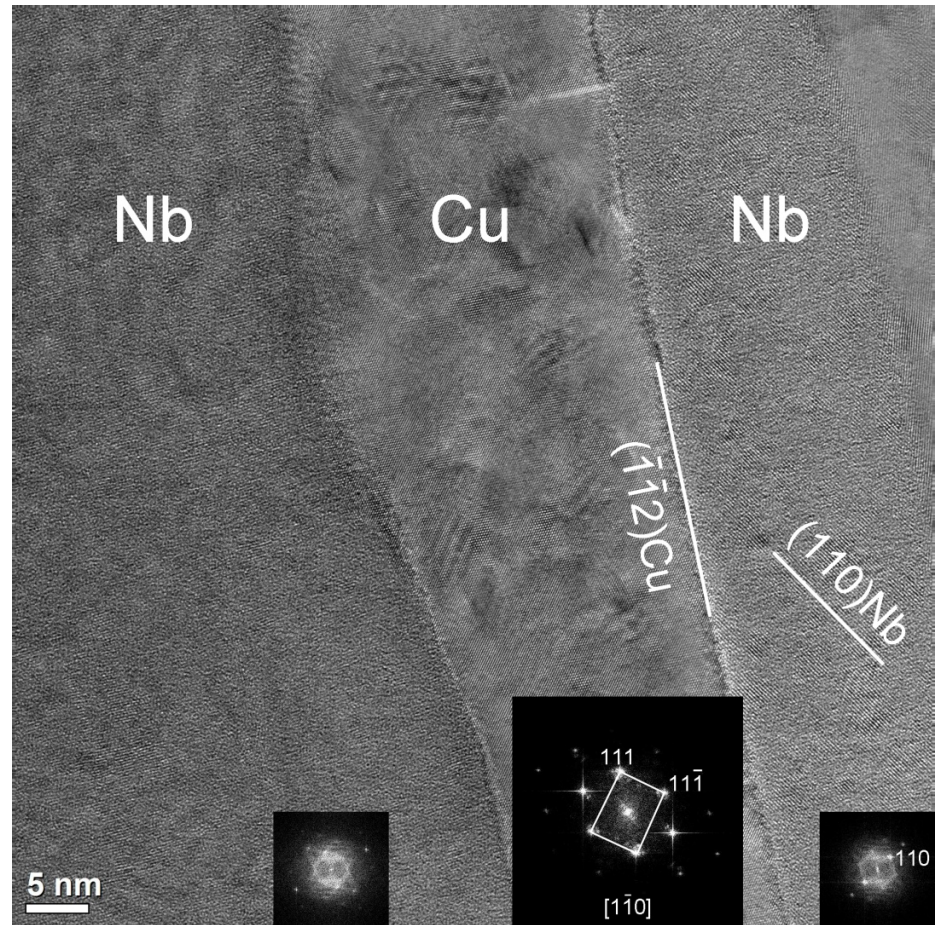
- Used drop furnace – each sample held for 1 hr at temperature in vacuum ( $10^{-7}$  Torr) and then furnace cooled
- Compare to conventional K-S ( $\{111\}$ Cu// $\{110\}$ Nb) interface,  $\{112\}$  K-S is high energy interface, is it thermally stable?
- Does the interface deviate from  $\{112\}$  K-S stable?
- Is a triple junction stable?
- Is a very thin layer stable?



{112} K-S interface is thermally stable



Interfaces that deviate from {112} K-S thermally unstable



# Widmanstätten morphology

- Widmanstätten's name is associated with platy precipitates that possess a definite crystallographic relationship with their parent phase.
- Examples:
  - ferrite in austenite (iron-rich meteors!)
  - $\gamma'$  precipitates in Al-Ag (see fig. 3.42)
  - hcp Ti in bcc Ti (two-phase Ti alloys, slow cooled)
  - $\theta'$  precipitates in Al-Cu
- The latter example is based on the orientation relationship  $(001)_{\theta'} // \{001\}_{Al}$ ,  $[100]_{\theta'} // \langle 100 \rangle_{Al}$ . See fig. 3.41 for a diagram of the tetragonal structure of  $\theta'$  whose  $a$ - $b$  plane, i.e.  $(001)$ , aligns with the  $(100)$  plane of the parent Al.

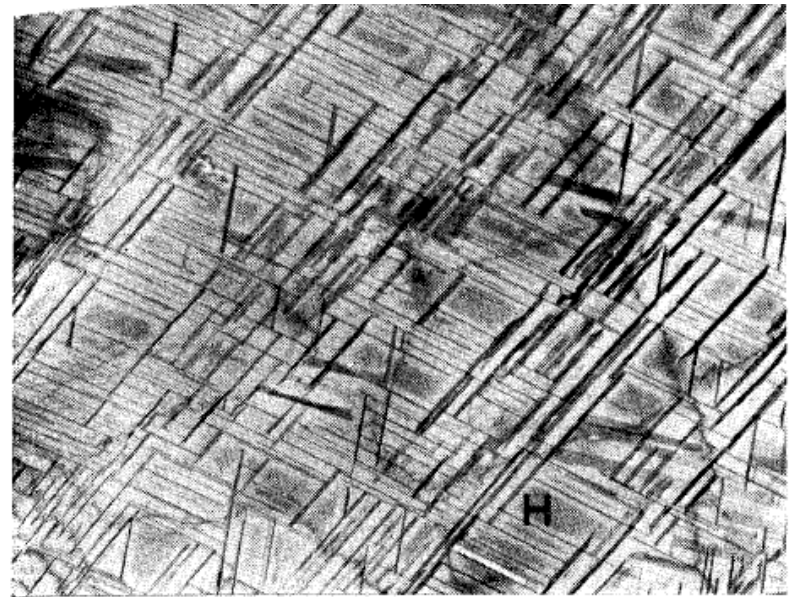


Fig. 3.42. Electron micrograph showing the Widmanstätten morphology of  $\gamma'$  precipitates in an Al-4 atomic % Ag alloy. GP zones can be seen between the  $\gamma'$ , e.g. at H ( $\times 7000$ ). (R.B. Nicholson and J. Nutting, *Acta Metallurgica*, **9** (1961) 332.)

# The Basics

Orientation relationships describe the specific orientation between two crystals

This is usually done for phase boundaries, but can describe grain boundaries as well.

Can you think of a special grain boundary that has a well-known orientation relationship?

$$(111)_\alpha // (111)_\beta$$

$$[0\bar{1}\bar{1}]_\alpha // [\bar{1}10]_\beta$$

The  $\Sigma 3$  CSL boundary has this OR. What is the habit plane if this is a coherent  $\Sigma 3$ ? Answer:  $\{111\}$



# Some common ORs

Bagaryatsky OR

$$\begin{aligned} [1\ 0\ 0]_{\text{cem}} \parallel [0\ -1\ 1]_{\text{fer}} \\ [0\ 0\ 1]_{\text{cem}} \parallel [-1\ -1\ 2]_{\text{fer}} \end{aligned}$$

Between cementite and ferrite phases in Pearlite.

Kurdjumov-Sachs OR

$$\begin{aligned} \{111\}_{\text{FCC}} \parallel \{0\ 1\ 1\}_{\text{BCC}} \\ \langle 101 \rangle_{\text{FCC}} \parallel \langle 1\ 1\ 1 \rangle_{\text{BCC}} \end{aligned}$$

Between austenite and ferrite phases in Iron; Cu-Zn.

Burgers OR

$$\begin{aligned} (0\ 0\ 0\ 1)_{\text{HCP}} \parallel \{0\ 1\ 1\}_{\text{BCC}} \\ [1\ 1\ -2\ 0]_{\text{HCP}} \parallel \langle 1\ 1\ 1 \rangle_{\text{BCC}} \end{aligned}$$

Between alpha and beta phases in Ti, Zr.

Potter OR

$$\begin{aligned} (0\ 1\ -1\ 1)_{\text{HCP}} \parallel \{-1\ 0\ 1\}_{\text{BCC}} \\ [2\ -1\ -1\ 0]_{\text{HCP}} \parallel \langle 1\ -1\ 1 \rangle_{\text{BCC}} \end{aligned}$$

Between alpha and beta phases in Mg-Al alloys.

# Complex semi-coherent interfaces

- It can often happen that an orientation relationship exists despite the lack of an exact match.
- Such is the case for the relationship between bcc and fcc iron (ferrite and austenite).

*Note limited atomic match for the NW relationship*

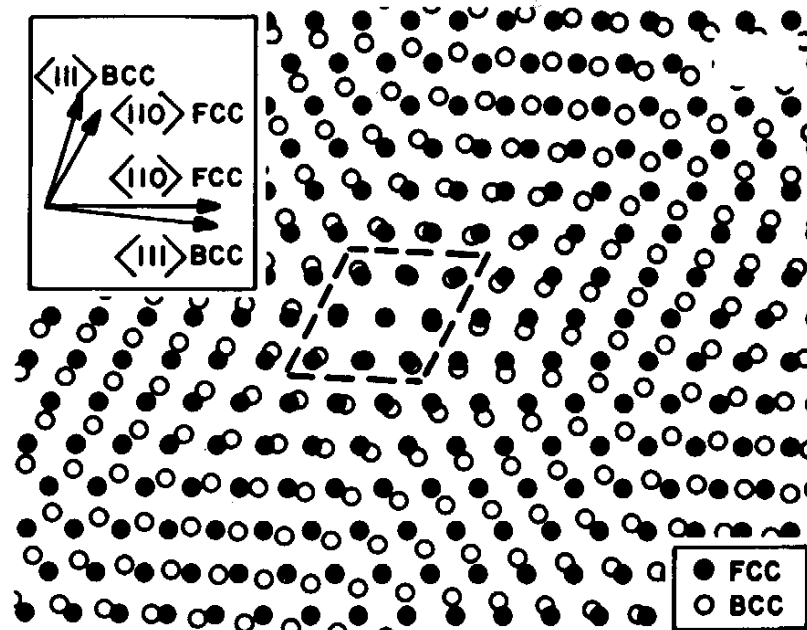


Fig. 3.38 Atomic matching across a  $(111)_{fcc}/(110)_{bcc}$  interface bearing the NW orientation relationship for lattice parameters closely corresponding to the case of fcc and bcc iron (M.G. Hall *et al.*, *Surface Science*, **31** (1972) 257).

\*Slide courtesy of AD Rollett

# Creating Coordinate Transformation Matrix for OR

Let's say you are given an orientation relationship and you want to know the rotation and change in volume between the two crystals. The coordinate transformation matrix,  $J$ , contains both pieces of information.

Given:  $(hkl)_\alpha // (h'k'l')_\beta$ ,  $[uvw]_\alpha // [u'v'w']_\beta$

First, define which phase is the parent phase and which is the derivative phase (e.g.  $\alpha \rightarrow \beta$ )

Define:

$$m = |(h \ k \ l)_\alpha| / |(h' \ k' \ l')_\beta|$$

$$k = |[u \ v \ w]_\alpha| / |[u' \ v' \ w']_\beta|$$

$$g = |[r \ s \ t]_\alpha| / |[r' \ s' \ t']_\beta|$$

Where did  $[rst]_\alpha$  and  $[r's't']_\beta$  come from?

Can either be specified in OR or found by cross product of normal vector,  $n$ , for  $(hkl)$  and direction vector,  $b$ , for  $[uvw]$ . (See earlier lectures for defining orientation matrix from  $(hkl)[uvw]$ .)

\*\* $k$ ,  $m$ , and  $g$  relate the length of the lattice vectors of the two crystals.



# Creating Coordinate Transformation Matrix for OR

Recall from previous lectures, each column represents the components of a basis vector of  $\alpha$  in  $\beta$ , in  $[uvw]$ ,  $[rst]$ ,  $(hkl)$  order.

To find  $J$  for  $\alpha \rightarrow \beta$ :

$$\begin{matrix} & \underline{\beta} & & & \underline{\alpha} \\ \left( \begin{array}{ccc} u' \cdot k & r' \cdot g & h' \cdot m \\ v' \cdot k & s' \cdot g & k' \cdot m \\ w' \cdot k & t' \cdot g & l' \cdot m \end{array} \right) & = J \times & \left( \begin{array}{ccc} u & r & h \\ v & s & k \\ w & t & l \end{array} \right) \end{matrix}$$

$$J = \left( \begin{array}{ccc} u' \cdot k & r' \cdot g & h' \cdot m \\ v' \cdot k & s' \cdot g & k' \cdot m \\ w' \cdot k & t' \cdot g & l' \cdot m \end{array} \right) \times \left( \begin{array}{ccc} u & r & h \\ v & s & k \\ w & t & l \end{array} \right)^{-1}$$

# Coordinate Transformation Matrix for OR to Strain<sup>68</sup> and Rotation Matrices

Within the transformation matrix are stretch,  $P$ , and rotation,  $U$ , matrices. When multiplied together these matrices recover the transformation matrix.  $J=UP$

To find the stretch and rotation matrices use a *polar decomposition*<sup>†</sup>.

$$P = \sqrt{J^* J}, \quad J^* \text{ denotes the conjugate transpose of } J$$

and 
$$U = J \cdot P^{-1}$$

Per usual, transform rotation matrix,  $U$ , to other notations for other uses

*\*\*Use MATLAB (function “poldec”) or some other computation package to make this calculation easier\*\**

<sup>†</sup>See, e.g., An Introduction to Continuum Mechanics, M. Gurtin

# Coordinate Transformation Matrix for OR to Strain and Rotation Matrices (Example) <sup>69</sup>

Given the Kurdjumov-Sachs OR for ferrite,  $\alpha$ , and austenite,  $\gamma$ , below, find the rotation matrix.

$$[1 \ 1 \ 1]_{\gamma} \parallel [0 \ 1 \ 1]_{\alpha} \qquad [\bar{1} \ 0 \ 1]_{\gamma} \parallel [\bar{1} \ \bar{1} \ 1]_{\alpha} \qquad [1 \ \bar{2} \ 1]_{\gamma} \parallel [2 \ \bar{1} \ 1]_{\alpha}$$

$$k = \frac{a_{\gamma} \sqrt{3}}{a_{\alpha} \sqrt{2}}$$

$$g = \frac{a_{\gamma} \sqrt{2}}{a_{\alpha} \sqrt{3}}$$

$$m = \frac{a_{\gamma} \sqrt{6}}{a_{\alpha} \sqrt{6}} = \frac{a_{\gamma}}{a_{\alpha}}$$

$$\begin{pmatrix} 0 & \bar{g} & 2m \\ k & \bar{g} & \bar{m} \\ k & g & m \end{pmatrix} = J \times \begin{pmatrix} 1 & \bar{1} & 1 \\ 1 & 0 & \bar{2} \\ 1 & 1 & 1 \end{pmatrix}$$

$$J = \frac{1}{6} \begin{pmatrix} 3g + 2m & \bar{4}m & \bar{3}g + 2m \\ 2k + 3g - m & 2k + 2m & 2k - 3g - m \\ 2k - 3g + m & 2k - 2m & 2k + 3g + m \end{pmatrix}$$

# Coordinate Transformation Matrix for OR to Strain<sup>70</sup> and Rotation Matrices (Example)

Given:  $a_\alpha = 0.28662$  nm  $a_\gamma = 0.36551$  nm

$$J = \begin{pmatrix} 0.9457 & -0.8502 & -0.0955 \\ 0.8287 & 0.9457 & -0.2125 \\ 0.2125 & 0.0955 & 1.2538 \end{pmatrix}$$

Polar Decomposition

$$U = \begin{pmatrix} 0.7416 & -0.6667 & -0.0749 \\ 0.6598 & 0.7416 & -0.1667 \\ 0.1667 & 0.0749 & 0.9832 \end{pmatrix} \quad \begin{matrix} \text{Rotation} \\ \text{Stretch} \end{matrix}$$
$$P = \begin{pmatrix} 1.2752 & 0.0000 & 0.0000 \\ 0.0000 & 1.2752 & 0.0000 \\ 0.0000 & 0.0000 & 1.2752 \end{pmatrix}$$

$$\text{Strain} = P - 1$$

# Summary

- Specific OR exists between product and parent phases for most of the transformations
- Well defined ORs also occur for thin film deposition
- Construction of misorientation matrix given an OR is straight-forward given parallel (hkl) [uvw]
- Some variants of an OR may be preferred over others depending on mechanism